

DESIGN AND IMPLEMENTATION OF A FLIGHT CONTROL SYSTEM FOR AN UNMANNED ROTORCRAFT USING RPT CONTROL APPROACH

Guowei Cai, Biao Wang, Ben M. Chen, and Tong H. Lee

ABSTRACT

In this paper, we apply a so-called robust and perfect tracking (RPT) control technique to the design and implementation of the flight control system of a miniature unmanned rotorcraft, named HeLion. To make the presented work self-contained, we will first outline some background knowledge, including mainly the nonlinear flight dynamics model and the inner-loop flight control system design. Next, the highlight of this paper, that is, the outer-loop flight control system design procedure using RPT control technique, will be detailed. Generally speaking, RPT control technique aims to design a controller such that (i) the resulting closed-loop system is asymptotically stable, and (ii) the controlled output almost perfectly tracks a given reference signal in the presence of any initial conditions and external disturbances. Since it makes use of all possible information including the system measurement output and the command reference signal together with all its derivatives (if available) for control, RPT control technique is particularly useful for the outer-loop layer of an unmanned aircraft. Both simulation and flight-test results will be presented and analyzed at the end of this paper, and the efficiency of the RPT control approach will be evaluated comprehensively.

Key Words: Unmanned aerial vehicles, flight control systems, robust control, tracking control.

I. INTRODUCTION

During the last two decades, miniature unmanned-aerial-vehicle (UAV) helicopters have gained great attention in academic circles worldwide. Some unique features such as low cost, good maneuverability, and easy maintenance, make them an ideal experimental platform for various research purposes. Their growing popularity in the last several years has been further revealed by some successful and impressive implementations (see, for example, [1,12,23,29]). The automatic flight control system is essential for a UAV to carry out flight missions with minimal or even without interference from human pilots. The classical single-input/single-output (SISO) feedback control method (i.e., PD or PID control) is one of the most common choices because of its simplicity in structure with less requirement on the accuracy of the dynamical model of the UAV. Examples include the CMU-R50 UAV helicopter [24], in which a SISO PD control law is adopted and further optimized using

CONDUIT for both hovering and forward flight, and the Ursa Major 3 UAV helicopter [27], in which a SISO PID control is implemented for automatic hovering. To improve flight control performance, many researchers are devoted to the study of implementing more advanced control techniques on the miniature rotorcraft UAVs. For example, a flight control system using a MIMO (multi-input/multi-output) H_∞ control approach has been designed and implemented for their mini rotorcraft UAVs in [34]. It is reported that the resulting system has clearly outperformed the classical method. Other cases reported in the literature include systems designed by using: (i) a decentralized decoupled model predictive approach [28]; (ii) a neural network method [15,32]; (iii) adaptive control techniques [11,22]; (iv) a fuzzy logic approach [20]; (v) μ -synthesis [33]; (vi) an approximate linearization method [21]; (vii) nonlinear control methods [3,26]; (viii) a differential geometry technique [19]; (ix) H_∞ control [16,17]; (x) a learning control technique [14]; (xi) intelligent control methods [31]; and (xii) a sliding mode control technique [13], to name a few. After decades of development, although there is a vast number of works that have been performed along these lines, many are still in the simulation stage. They are still not ready for reliable and mature implementations onto real platforms.

Recently, Cai et al. [4,5] (see also Peng et al. [25]) have proposed a flight control scheme consisting of three parts,

Manuscript received March 7, 2011; revised September 5, 2011; accepted November 6, 2011.

Guowei Cai is with Temasek Laboratories, National University of Singapore, Singapore 117411.

Biao Wang, Ben M. Chen (corresponding author) and Tong H. Lee are with the Department of Electrical & Computer Engineering, National University of Singapore, Singapore 117576 (e-mails: tscaig@nus.edu.sg; elewb@nus.edu.sg; bmchen@nus.edu.sg; eleleeth@nus.edu.sg).

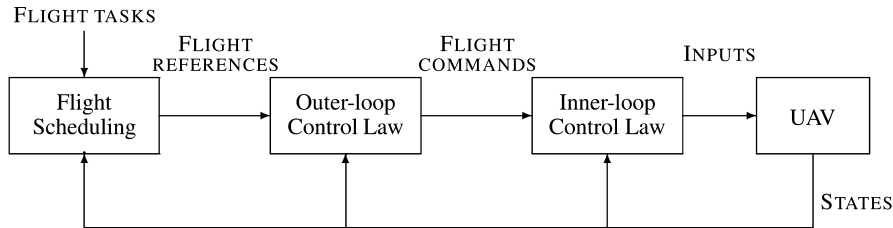


Fig. 1. Structure of the hierarchical flight control system.



Fig. 2. HeLion—a fully autonomous unmanned helicopter.

namely, the inner-loop control, outer-loop control and flight scheduling (see Fig. 1). In [4], the function of the inner-loop control law, designed using the H_∞ control approach, is to guarantee the asymptotic stability of the aircraft motion with respect to the surrounding air and to have good disturbance rejection with respect to wind gusts. The role of the outer-loop controller is to produce flight commands or references to the inner-loop control layer, and lastly, the task of the flight scheduling part is to generate the flight references for pre-scheduled flight missions.

We would like to note that the outer-loop layer reported in [4] consists of a set of simple proportional controllers for which it is hard to push their overall performance. In this paper, we propose the design of the outer-loop controllers for our unmanned helicopter system, HeLion [6] (see Fig. 2). HeLion is the first miniature unmanned rotorcraft constructed at National University of Singapore. Using a Raptor 90-SE hobby helicopter as the baseline, HeLion is equipped with a compact and light-weight avionic system (developed by our NUS UAV research team) to realize high-performance fully autonomous flight. More specifically, the design method to be implemented is the

so-called robust and perfect tracking (RPT) control technique. It was developed by Chen and his co-workers (see, e.g., [9,10]) and is capable of achieving much better performance for situations when complicated maneuvers are required. The robust and perfect tracking control technique is to design a controller such that the resulting closed-loop system is asymptotically stable and the controlled output almost perfectly tracks a given reference signal in the presence of any initial conditions and external disturbances. It makes use of all possible information including the system measurement output and the command reference signal together with all its derivatives, if available, for control. Such a unique feature is particularly useful for the outer-loop layer, in which the position reference and its velocity, as well as acceleration, all can be measured by the onboard avionic system. Our design has been successfully demonstrated in both simulation and actual flight tests. In fact, the flight control system within the RPT control framework renders the flight formation of multiple UAVs a trivial task, *i.e.*, there is no need to design an additional controller for realizing flight formation of multiple vehicles.

The outline of this paper is as follows. In Section II, we briefly introduce some background material on the dynamic model of the unmanned rotorcraft and the inner-loop controller of the flight control system. Section III presents the RPT control technique and the detailed design procedure for the outer-loop controllers of the unmanned system, and Section IV gives the performance evaluation of our design through simulation and actual flight test results in a wide-envelope flight mission. Finally, we draw some concluding remarks in Section V.

II. BACKGROUND MATERIAL

It is crucial to obtain a fairly comprehensive model of a UAV if one wishes to design an advanced automatic flight control system by incorporating advanced control techniques. In this section, we briefly recall the flight dynamics model structure for HeLion and its associated inner-loop controller designed using the H_∞ control method. As the main focus of this paper is on the outer layer of the automatic flight control

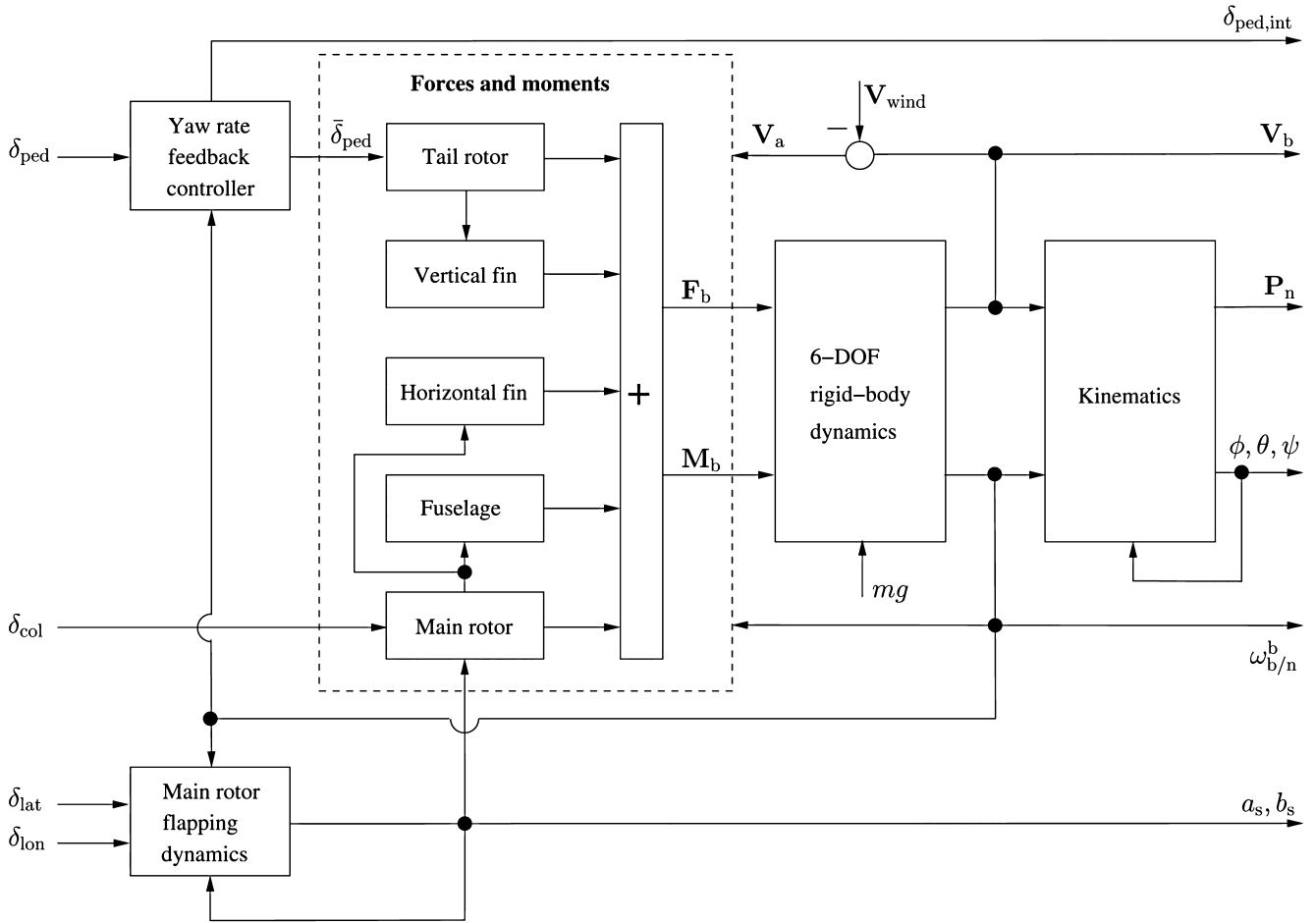


Fig. 3. Structure of the HeLion dynamic model.

system, we refer interested readers to necessary references for more detailed information on the topics highlighted in this section.

2.1 Dynamic model of the unmanned rotorcraft

We have obtained a complete flight dynamics model for HeLion in [8] using the first-principles approach. The complete structure of the nonlinear model is depicted in Fig. 3, which includes four key components: (i) kinematics; (ii) 6-DOF rigid-body dynamics; (iii) main rotor flapping dynamics; and (iv) factory-installed yaw rate feedback controller dynamics. This flight dynamics model features minimum complexity and contains fifteen states and four inputs, which are illustrated in Fig. 4 and summarized in Table I. In the modeling procedure, some unique features of the hobby-based helicopters, such as stabilizer bar configuration and the yaw rate feedback controller, have been included. The necessity has been well proven in some documented work (see, for example, [8,24]).

2.1.1 Kinematics

The Kinematics part includes two equations, which describe the relative motions between the two coordinate frames adopted, *i.e.*, the body frame and the local north-east-down (NED) frame. More specifically, the one relative to the translational motion is given by

$$\dot{\mathbf{P}}_n = \mathbf{V}_n = \mathbf{R}_{n/b} \mathbf{V}_b, \tag{1}$$

and the relative rotational motion is expressed by

$$\begin{pmatrix} \dot{\phi} \\ \dot{\theta} \\ \dot{\psi} \end{pmatrix} = \mathbf{S}^{-1} \boldsymbol{\omega}_{b/n}^b, \tag{2}$$

where \mathbf{P}_n is the NED-based position vector, \mathbf{V}_n is the NED-based velocity vector, \mathbf{V}_b is the body-frame velocity vector, $\boldsymbol{\omega}_{b/n}^b$ is the angular rate vector, $\mathbf{R}_{n/b}$ and \mathbf{S} are the

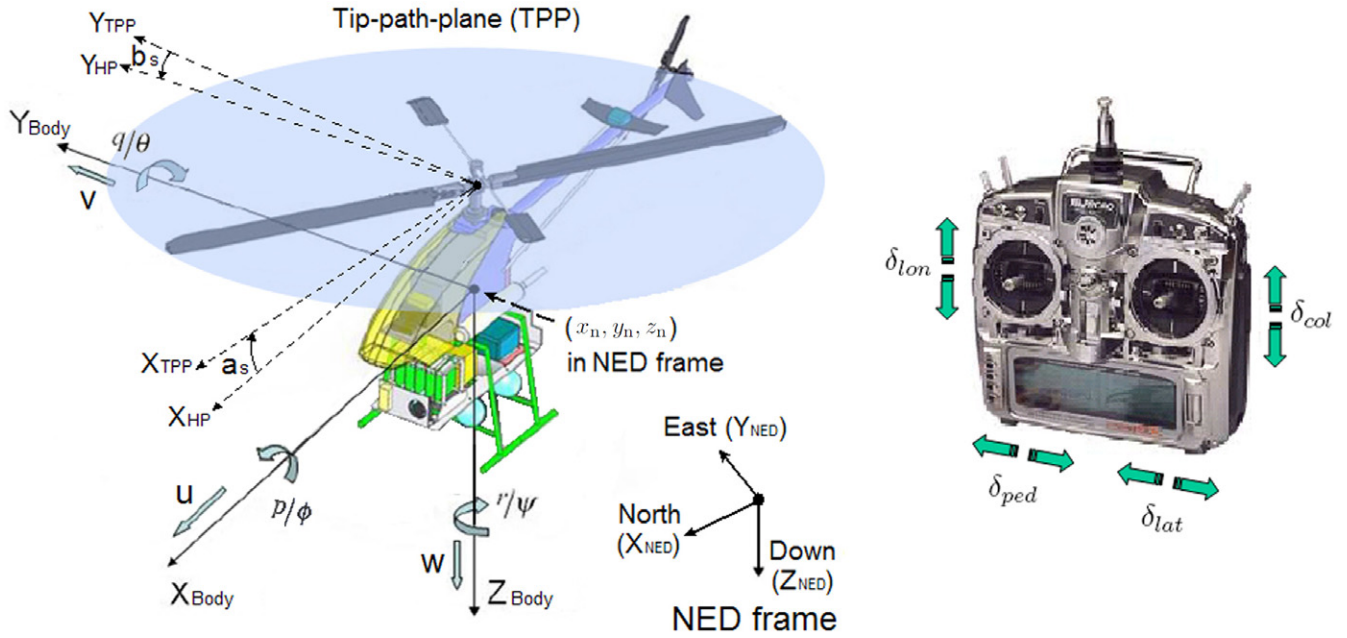


Fig. 4. Illustration of the state and input variables.

Table I. Physical meanings of the state and input variables.

| Variable | Physical meaning | Unit |
|----------------------|--|-------|
| x_n, y_n, z_n | Variables of NED-frame position \mathbf{P}_n | m |
| u, v, w | Variables of body-frame velocity \mathbf{V}_b | m/s |
| p, q, r | Roll, pitch, yaw angular rates of vector $\boldsymbol{\omega}_{b/n}^b$ | rad/s |
| ϕ, θ, ψ | Roll, pitch, yaw angles | rad |
| a_s | Longitudinal tip-path-plane (TPP) flapping angle | rad |
| b_s | Lateral TPP flapping angle | rad |
| δ_{ped}^{int} | Intermediate state in yaw rate feedback controller dynamics | NA |
| δ_{lat} | Normalized aileron servo input (-1 ~ 1) | NA |
| δ_{on} | Normalized elevator servo input (-1 ~ 1) | NA |
| δ_{col} | Normalized collective pitch servo input (-1 ~ 1) | NA |
| δ_{ped} | Normalized rudder servo input (-1 ~ 1) | NA |

transformation matrices and are, respectively, given as (see also, e.g., [30]):

$$\mathbf{R}_{n/b} = \begin{bmatrix} \cos \theta \cos \psi & \sin \phi \sin \theta \cos \psi - \cos \phi \sin \psi \\ \cos \theta \sin \psi & \sin \phi \sin \theta \sin \psi + \cos \phi \cos \psi \\ -\sin \theta & \sin \phi \cos \theta \\ \cos \phi \sin \theta \cos \psi + \sin \phi \sin \psi \\ \cos \phi \sin \theta \sin \psi - \sin \phi \cos \psi \\ \cos \phi \cos \theta \end{bmatrix} \quad (3)$$

and

$$\mathbf{S}^{-1} = \begin{bmatrix} 1 & \sin \phi \tan \theta & \cos \phi \tan \theta \\ 0 & \cos \phi & -\sin \phi \\ 0 & \sin \phi / \cos \theta & \cos \phi / \cos \theta \end{bmatrix}. \quad (4)$$

2.1.2 Rigid-body dynamics

Assuming that the local NED coordinate is inertial, the rigid-body dynamics of a UAV helicopter is represented by the following Newton-Euler equations

$$\dot{\mathbf{V}}_b = -\boldsymbol{\omega}_{b/n}^b \times \mathbf{V}_b + \frac{\mathbf{F}_b}{m} + \frac{\mathbf{F}_{b,g}}{m} \quad (5)$$

and

$$\dot{\boldsymbol{\omega}}_{b/n}^b = \mathbf{J}^{-1} [\mathbf{M}_b - \boldsymbol{\omega}_{b/n}^b \times (\mathbf{J} \boldsymbol{\omega}_{b/n}^b)], \quad (6)$$

where “ \times ” denotes the cross-product of two vectors, m is the mass of the helicopter, $\mathbf{F}_{b,g}$ is the gravity force vector projected onto the body frame, $\mathbf{J} = \text{diag}\{J_{xx}, J_{yy}, J_{zz}\}$ is the diagonal moment of inertia matrix. We need to highlight that \mathbf{F}_b and \mathbf{M}_b are the combined aerodynamic force and moment vectors, which are generated by (i) the main rotor, (ii) tail rotor, (iii) fuselage, (iv) vertical fin, and (v) horizontal fin. The detailed expressions can be found in [8,18].

2.1.3 Main rotor flapping dynamics

For small-scale helicopters, the main rotor is commonly augmented by a stabilizer bar to enhance the human control

stability while maintaining the maneuverability. The dynamics of the stabilizer bar can be lumped into that of the bare main rotor, and the augmented flapping dynamics can be described by the following two coupled first-order differential equations:

$$\dot{a}_s = -q - \frac{1}{\tau_{\text{eff}}} a_s + \frac{A_{b_s}}{\tau_{\text{eff}}} b_s + \frac{A_{\text{lon}}}{\tau_{\text{eff}}} \delta_{\text{lon}} \quad (7)$$

and

$$\dot{b}_s = -p + \frac{B_{a_s}}{\tau_{\text{eff}}} a_s - \frac{1}{\tau_{\text{eff}}} b_s + \frac{B_{\text{lat}}}{\tau_{\text{eff}}} \delta_{\text{lat}}, \quad (8)$$

where τ_{eff} is the effective time constant of the augmented main rotor system which counts for the stabilizer bar, A_{b_s} and B_{a_s} are the coupling effect between longitudinal and lateral flapping motions, and A_{lon} and B_{lat} are the effective linkage gains.

2.1.4 Yaw rate feedback controller dynamics

To the human control of the miniature helicopters, a yaw rate feedback controller is required to assist the pilot to deal with the high sensitivity of the bare yaw channel dynamics. This feature is retained when we upgrade a hobby helicopter to an UAV system. Considering the feedback controller is a PI type, we first define an intermediate state $\delta_{\text{ped,int}}$, which is the integration of the error between the amplified yaw channel input signal and the yaw rate feedback, with

$$\dot{\delta}_{\text{ped,int}} = K_a \delta_{\text{ped}} - r, \quad (9)$$

and then express the PI relationship as

$$\bar{\delta}_{\text{ped}} = K_p (K_a \delta_{\text{ped}} - r) + K_I \delta_{\text{ped,int}}, \quad (10)$$

where K_p and K_I are the proportional and integral gains of the embedded controller, K_a is the scaling value of the embedded amplifier circuit, and $\bar{\delta}_{\text{ped}}$ is the actual rudder servo actuator deflection for generating the tail rotor force and moment.

Among the aforementioned ten equations, (1, 2, 5, 6, 7, 8, 9) contain the fifteen states listed in Table I and can form a state-space structure. In [8], we have provided a detailed procedure to determine the model parameters of HeLion. The model we have obtained has been proven to be highly accurate. We refer interested readers to [8] for the detailed identification procedure and identified parameters.

2.2 Inner-loop flight control system

As mentioned earlier, we will adopt the three-layer automatic flight control system as given in Fig. 1 for our unmanned vehicles based on the time scales of the state variables of the helicopter. The detailed structure of the inner-loop layer and the outer-loop layer of our automatic flight control system is depicted in Fig. 5, in which:

1. the inner loop stabilizes the dynamics of the helicopter associated with its Euler angles ϕ , θ , and ψ , angular velocities p , q , and r , tip-path-plane (TPP) flapping angles of the main rotor a_s and b_s , and the intermediate state of the built-in yaw rate feedback controller $\delta_{\text{ped,int}}$; and
2. the outer loop controls the local-NED-based positions x_n , y_n , and z_n , and their respective velocities u_n , v_n , and w_n . Generally, the dynamics associated with the outer-loop layer are much slower compared to those in the inner loop.

In [4], the H_∞ control technique is employed to design an inner-loop control law for HeLion. In the adopted three-layer flight control structure, it turns out that the inner-loop dynamics model is almost invariant with respect to the flight velocities. Here we need to highlight that (i) the invariability of the inner-loop dynamics only holds when a miniature rotorcraft performs non-acrobatic maneuvers (*i.e.*, without drastic changes in attitude dynamics), and (ii) despite the invariance of the parameters of the inner-loop dynamics model, the trimmed values of both input and state variables (defined respectively by \mathbf{u}_{trim} and \mathbf{x}_{trim}) show a notable change subject to a different flight velocity. The unified linearized model for the inner loop is given by

$$\dot{\mathbf{x}}_{\text{in}} = A\mathbf{x}_{\text{in}} + B\mathbf{u}_{\text{in}} + E\mathbf{w}_{\text{in}}, \quad (11)$$

where \mathbf{w}_{in} is the wind gust disturbance, $\mathbf{x}_{\text{in}} = \mathbf{x}_{\text{act}} - \mathbf{x}_{\text{trim}}$ is the difference between the actual state variables and their trimmed values, and similarly, $\mathbf{u}_{\text{in}} = \mathbf{u}_{\text{act}} - \mathbf{u}_{\text{trim}}$ is the difference between the actual input variables and their trimmed values, and where \mathbf{x}_{act} and \mathbf{u}_{act} are respectively given as

$$\mathbf{x}_{\text{act}} = [\phi \quad \theta \quad p \quad q \quad a_s \quad b_s \quad r \quad \delta_{\text{ped,int}} \quad \psi]^T \quad (12)$$

and

$$\mathbf{u}_{\text{act}} = [\delta_{\text{lat}} \quad \delta_{\text{lon}} \quad \delta_{\text{ped}}]^T. \quad (13)$$

Moreover, A , B and E for HeLion are respectively given by

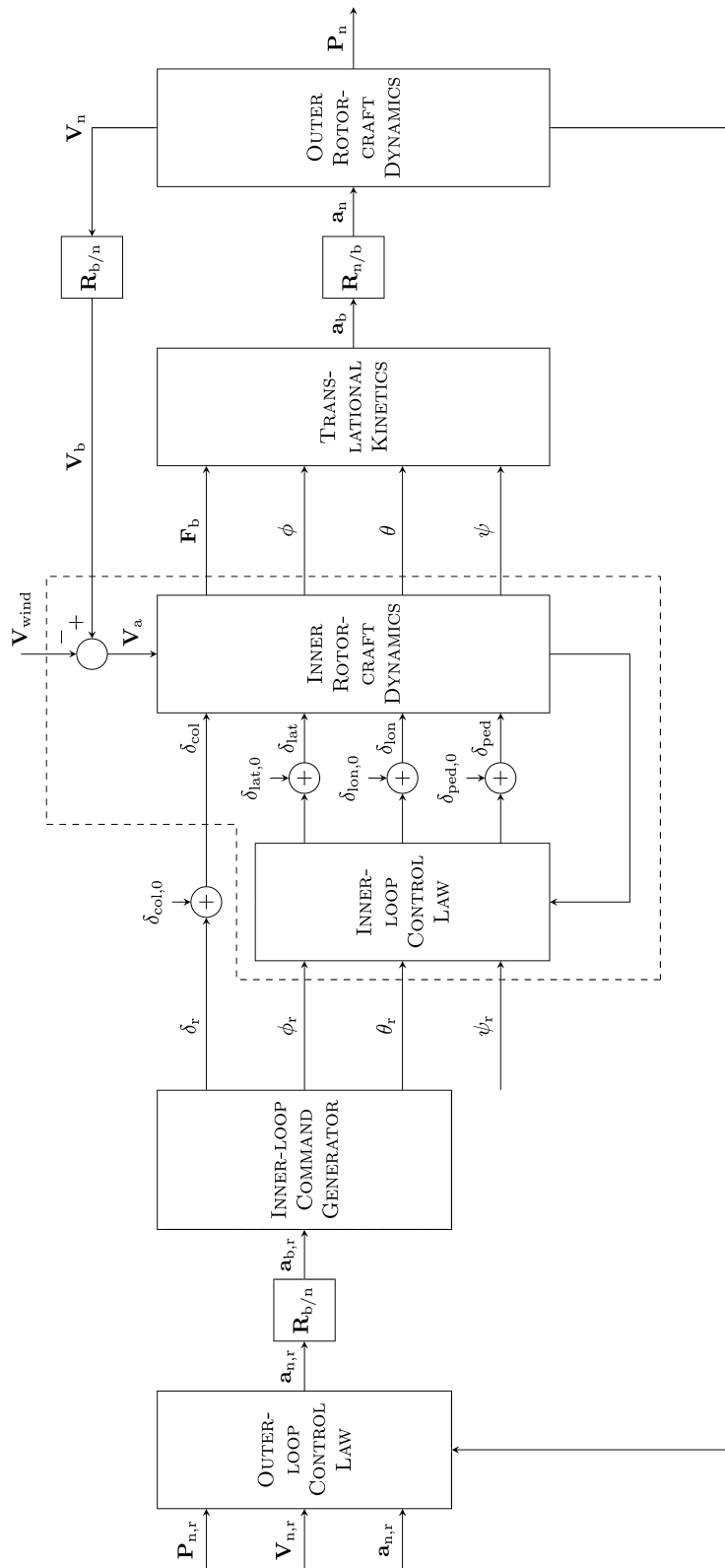


Fig. 5. Detailed structure of the inner-loop and outer-loop layers of the flight control system.

$$A = \begin{bmatrix} 0 & 0 & 1 & 0 & 0 \\ 0 & 0 & 0 & 0.9992 & 0 \\ 0 & 0 & -0.0302 & -0.0056 & -0.003 \\ 0 & 0 & 0 & -0.0707 & 267.7499 \\ 0 & 0 & 0 & -1.0000 & -3.3607 \\ 0 & 0 & -1 & 0 & 2.4483 \\ 0 & 0 & 0.0579 & 0.0108 & 0.0049 \\ 0 & 0 & 0 & 0 & 0 \\ 0 & 0 & 0 & 0.0389 & 0 \\ 0 & 0.0009 & 0 & 0 & 0 \\ 0 & -0.0389 & 0 & 0 & 0 \\ 585.1165 & 11.4448 & -59.529 & 0 & 0 \\ -0.0003 & 0 & 0 & 0 & 0 \\ 2.2223 & 0 & 0 & 0 & 0 \\ -3.3607 & 0 & 0 & 0 & 0 \\ 0.0037 & -21.9557 & 114.2 & 0 & 0 \\ 0 & -1 & 0 & 0 & 0 \\ 0 & 0.9992 & 0 & 0 & 0 \end{bmatrix}$$

and

$$B = \begin{bmatrix} 0 & 0 & 0 \\ 0 & 0 & 0 \\ 0 & 0 & 43.3635 \\ 0 & 0 & 0 \\ 0.2026 & 2.5878 & 0 \\ 2.5878 & -0.0663 & 0 \\ 0 & 0 & -83.1883 \\ 0 & 0 & -3.8500 \\ 0 & 0 & 0 \\ 0 & 0 & 0 \\ 0 & 0 & 0 \\ -0.0001 & 0.1756 & -0.0395 \\ 0.0000 & 0.0003 & 0.0338 \\ 0 & 0 & 0 \\ 0 & 0 & 0 \\ -0.0002 & -0.3396 & 0.6424 \\ 0 & 0 & 0 \\ 0 & 0 & 0 \end{bmatrix},$$

$$E = \begin{bmatrix} 0 & 0 & 0 \\ 0 & 0 & 0 \\ 0 & 0 & 0 \\ 0 & 0 & 0 \\ 0 & 0 & 0 \\ 0 & 0 & 0 \\ 0 & 0 & 0 \\ 0 & 0 & 0 \\ 0 & 0 & 0 \\ 0 & 0 & 0 \\ 0 & 0 & 0 \\ 0 & 0 & 0 \\ 0 & 0 & 0 \\ 0 & 0 & 0 \\ 0 & 0 & 0 \\ 0 & 0 & 0 \\ 0 & 0 & 0 \\ 0 & 0 & 0 \end{bmatrix}.$$

The measurement output is given by

$$\mathbf{y} = [\phi \ \theta \ p \ q \ r \ \psi]^T - \mathbf{y}_{\text{trim}}, \quad (14)$$

where \mathbf{y}_{trim} is the trim value of the corresponding measurable state variables. The primary output to be controlled is selected as

$$\mathbf{h} := [\phi \ \theta \ \psi]^T - \mathbf{h}_{\text{trim}}, \quad (15)$$

where \mathbf{h}_{trim} is the trim value of the corresponding \mathbf{h} . Under this problem formulation setting and using the technique for general H_∞ control given in [9], an effective inner-loop controller has been obtained and is given as the following:

$$\mathbf{u}_{\text{in}} = F\hat{\mathbf{x}}_{\text{in}} + G(\mathbf{r} - \mathbf{h}_{\text{trim}}), \quad (16)$$

where $\mathbf{r} = [\phi_r \ \theta_r \ \psi_r]^T$ is the reference signal vector generated by a command generator linked to the outer-loop control law,

$$F = \begin{bmatrix} -1.0368 & -0.0604 & -0.0230 & -0.0083 & -0.2857 \\ 0.0760 & -0.9970 & 0.0174 & -0.0378 & -1.8340 \\ -0.0002 & -0.0185 & -0.0066 & 0.0004 & 0.0353 \\ -2.6165 & -0.0312 & 0.0499 & -0.0746 \\ -0.1130 & 0.0026 & 0.0024 & -0.0169 \\ 0.0990 & 0.0044 & 0.2295 & 0.2441 \end{bmatrix},$$

$$G = \begin{bmatrix} 1.0368 & 0.0604 & 0.0746 \\ -0.0760 & 0.9970 & 0.0169 \\ 0.0002 & 0.0185 & -0.2441 \end{bmatrix},$$

and $\hat{\mathbf{x}}_{\text{in}}$ is the estimation of the state variable \mathbf{x}_{in} . There are only three state variables, *i.e.*, a_s , b_s and $\delta_{\text{ped,int}}$, that cannot be directly measured. The estimation of \mathbf{x}_{in} can be done through the following reduced-order estimator:

$$\dot{\hat{\mathbf{x}}}_{\text{in,cmp}} = A_{\text{in,cmp}}\hat{\mathbf{x}}_{\text{in,cmp}} + B_{\text{in,cmp}}\mathbf{y} + H_{\text{in,cmp}}\mathbf{u}_{\text{in}}, \quad (17)$$

where

$$A_{\text{in,cmp}} = \begin{bmatrix} -10 & 0 & 0 \\ 0 & -10 & 0 \\ 0 & 0 & -12 \end{bmatrix},$$

$$H_{\text{in,cmp}} = \begin{bmatrix} 0.2026 & 2.5878 & 0 \\ 2.5878 & -0.0663 & 0 \\ 0 & 0 & 4.8913 \end{bmatrix},$$

$$B_{\text{in,cmp}} = 10^{-2} \times \begin{bmatrix} 0 & 0 & -3.7980 & -124.6213 & -1.9798 & 0 \\ 0 & 0 & -111.3469 & -9.0793 & -5.9148 & 0 \\ 0 & 0 & -0.6076 & -0.1112 & 4.6136 & 0 \end{bmatrix}.$$

The estimation of the unmeasurable state variables is given by

$$\begin{pmatrix} \hat{a}_s \\ \hat{b}_s \\ \hat{\delta}_{\text{ped,int}} \end{pmatrix} = \hat{\mathbf{x}}_{\text{in,cmp}} + K_{\text{in,cmp}}\mathbf{y}, \quad (18)$$

where

$$K_{\text{in,comp}} = 10^{-3} \times \begin{bmatrix} 0 & 0 & 3.7980 & 24.7966 & 1.9798 & 0 \\ 0 & 0 & 11.3469 & 9.1439 & 5.9148 & 0 \\ 0 & 0 & 0 & 0 & 105.0784 & 0 \end{bmatrix}.$$

It is shown that the above inner-loop control law is able to achieve the top level performance in all the categories under examination in accordance with the standards set for military rotorcraft by US Army Aviation [2].

III. OUTER-LOOP FLIGHT CONTROL SYSTEM

As mentioned earlier, the outer loop of our proposed automatic flight control system is for controlling the position of the unmanned system in the local NED frame. Traditionally, the outer-loop layer can be controlled by simple controllers, such as PID or even proportional control laws (see, e.g., [4]). However, the flight control system with simple outer-loop controllers can only provide reasonable performance for position and heading control. When it comes to situations in which complicated maneuvers are required, it generally results in poor performance. We propose in this chapter the design of the outer-loop controllers for our unmanned systems using the so-called robust and perfect tracking (RPT) control technique developed by Chen and his co-workers (see, e.g., [9,10]). Given a system that satisfies certain conditions, the RPT control technique is for designing a controller such that the resulting closed-loop system is asymptotically stable and the controlled output almost perfectly tracks a given reference signal in the presence of any initial conditions and external disturbances. Almost perfect tracking means the ability of a controller to track a given reference signal with an arbitrarily fast settling time in the face of external disturbances and initial conditions. Of course, in real life, a certain tradeoff has to be made in order to design a physically implementable control law.

We should highlight that one of the most interesting features in the RPT control method is its capability of utilizing all possible information available in its controller structure. More specifically, given a reference, if its derivatives are also available, all of them can be fed into the RPT controller to yield a better performance. Such a feature is highly desirable for flight missions involving complicated maneuvers, in which not only the position reference is useful, but also its velocity and even acceleration information are important or even necessary to be used in order to achieve a good overall performance. As a result, the RPT control renders the flight formation of multiple UAVs a trivial task. In what follows, we first recall the basic theory behind the RPT technique. Interested readers are referred to [9] for the rigorous treatment of the RPT control theory.

3.1 Robust and perfect tracking control under state feedback

Consider the following continuous-time system:

$$\Sigma: \begin{cases} \dot{x} = Ax + Bu + Ew, & x(0) = x_0, \\ y = x \\ h = C_2x + D_2u \end{cases} \quad (19)$$

where $x \in \mathbb{R}^n$ is the state, $u \in \mathbb{R}^m$ is the control input, $w \in \mathbb{R}^q$ is the external disturbance, and $h \in \mathbb{R}^l$ is the output to be controlled. Given the external disturbance $w \in L_p$, $p \in [1, \infty)$, and any reference signal vector $r \in \mathbb{R}^l$ with $r, \dot{r}, \dots, r^{(\kappa-1)}$, $\kappa \geq 1$, being available, and $r^{(\kappa)}$ being either a vector of delta functions or in L_p , the RPT problem for the system in (19) is to find a parameterized state feedback control law of the following form:

$$u = F(\varepsilon)x + H_0(\varepsilon)r + \dots + H_{\kappa-1}(\varepsilon)r^{(\kappa-1)} \quad (20)$$

such that when the controller of (20) is applied to the system of (19), we have the following:

1. There exists an $\varepsilon^* > 0$ such that the resulting closed-loop system with $r=0$ and $w=0$ is asymptotically stable for all $\varepsilon \in (0, \varepsilon^*)$.
2. Let $h(t, \varepsilon)$ be the closed-loop controlled output response and let $e(t, \varepsilon)$ be the resulting tracking error, i.e., $e(t, \varepsilon) = h(t, \varepsilon) - r(t)$. Then, for any initial condition of the state, $x_0 \in \mathbb{R}^n$,

$$\|e\|_p = \left(\int_0^\infty |e(t)|^p dt \right)^{1/p} \rightarrow 0 \quad \text{as } \varepsilon \rightarrow 0. \quad (21)$$

We introduce in the above formulation some additional information besides the reference signal r , i.e., $\dot{r}, \ddot{r}, \dots, r^{(\kappa-1)}$, as additional controller inputs. In flight control systems, taking r as a position reference, generally, its associated velocity, \dot{r} , and acceleration, \ddot{r} , are readily available. These $\dot{r}(t)$ and $\ddot{r}(t)$ can be used to improve the overall tracking performance. It was shown in [9] that the RPT problem for the system in (19) is solvable if and only if (i) (A, B) is stabilizable, and (ii) (A, B, C_2, D_2) is right invertible and of minimum phase.

In what follows, we construct a parameterized state feedback control law as given in (20) that solves the RPT problem for the system in (19). It is simple to note that we can rewrite the given reference in the following form:

$$\frac{d}{dt} \begin{pmatrix} r \\ \vdots \\ r^{(\kappa-2)} \\ r^{(\kappa-1)} \end{pmatrix} = \begin{bmatrix} 0 & I_\ell & \cdots & 0 \\ \vdots & \vdots & \ddots & \vdots \\ 0 & 0 & \cdots & I_\ell \\ 0 & 0 & \cdots & 0 \end{bmatrix} \begin{pmatrix} r \\ \vdots \\ r^{(\kappa-2)} \\ r^{(\kappa-1)} \end{pmatrix} + \begin{pmatrix} 0 \\ \vdots \\ \vdots \\ I_\ell \end{pmatrix} r^{(\kappa)}. \quad (22)$$

Combining (22) with the given system, we obtain the following augmented system:

$$\Sigma_{\text{AUG}}: \begin{cases} \dot{\mathbf{x}} = \mathbf{A}\mathbf{x} + \mathbf{B}u + \mathbf{E}w \\ \mathbf{y} = \mathbf{x} \\ e = \mathbf{C}_2\mathbf{x} + \mathbf{D}_2u \end{cases} \quad (23)$$

where

$$\mathbf{x} := \begin{pmatrix} r \\ \vdots \\ r^{(\kappa-2)} \\ r^{(\kappa-1)} \\ x \end{pmatrix}, \quad \mathbf{w} := \begin{pmatrix} w \\ r^{(\kappa)} \end{pmatrix}, \quad (24)$$

$$\mathbf{A} = \begin{bmatrix} 0 & I_\ell & \cdots & 0 & 0 \\ \vdots & \vdots & \ddots & \vdots & \vdots \\ 0 & 0 & \cdots & I_\ell & 0 \\ 0 & 0 & \cdots & 0 & 0 \\ 0 & 0 & \cdots & 0 & A \end{bmatrix}, \quad \mathbf{B} = \begin{bmatrix} 0 \\ \vdots \\ 0 \\ B \end{bmatrix}, \quad (25)$$

$$\mathbf{E} = \begin{bmatrix} 0 & 0 \\ \vdots & \vdots \\ 0 & 0 \\ 0 & I_\ell \\ E & 0 \end{bmatrix},$$

and

$$\mathbf{C}_2 = [-I_\ell \ 0 \ 0 \ \cdots \ 0 \ C_2], \quad \mathbf{D}_2 = D_2. \quad (26)$$

It is then straightforward to show that the subsystem from u to e in the augmented system of (23), *i.e.*, the quadruple $(\mathbf{A}, \mathbf{B}, \mathbf{C}_2, \mathbf{D}_2)$, is right invertible and has the same infinite zero structure as that of (A, B, C_2, D_2) . Furthermore, its invariant zeros contain those of (A, B, C_2, D_2) and $\ell \times \kappa$ extra ones at $s = 0$.

Next, we define

$$\tilde{\mathbf{C}}_2 = \begin{bmatrix} \mathbf{C}_2 \\ \epsilon I_{\kappa\ell+n} \\ 0 \end{bmatrix}, \quad \mathbf{D}_2 = \begin{bmatrix} \mathbf{D}_2 \\ 0 \\ \epsilon I_m \end{bmatrix}, \quad (27)$$

$$\tilde{\mathbf{A}} = \begin{bmatrix} \tilde{\mathbf{A}}_0 & 0 \\ 0 & A \end{bmatrix}, \quad \tilde{\mathbf{A}}_0 = -\epsilon_0 I_{\kappa\ell} + \begin{bmatrix} 0 & I_\ell & \cdots & 0 \\ \vdots & \vdots & \ddots & \vdots \\ 0 & 0 & \cdots & I_\ell \\ 0 & 0 & \cdots & 0 \end{bmatrix}, \quad (28)$$

where ϵ_0 is a sufficiently small scalar (introduced to fool the Riccati equation), and solve the following Riccati equation:

$$\tilde{\mathbf{P}}\tilde{\mathbf{A}} + \tilde{\mathbf{A}}^T\tilde{\mathbf{P}} + \tilde{\mathbf{C}}_2^T\tilde{\mathbf{C}}_2 - (\mathbf{P}\mathbf{B} + \tilde{\mathbf{C}}_2^T\tilde{\mathbf{D}}_2)(\tilde{\mathbf{D}}_2^T\tilde{\mathbf{D}}_2)^{-1}(\mathbf{P}\mathbf{B} + \tilde{\mathbf{C}}_2^T\tilde{\mathbf{D}}_2)^T = 0 \quad (29)$$

for a positive-definite solution $\mathbf{P} > 0$. The required state feedback gain matrix that solves the RPT problem for the given system is then given by

$$\tilde{\mathbf{F}}(\epsilon) = -(\tilde{\mathbf{D}}_2^T\tilde{\mathbf{D}}_2)^{-1}(\mathbf{P}\mathbf{B} + \tilde{\mathbf{C}}_2^T\tilde{\mathbf{D}}_2)^T \\ = [H_0(\epsilon) \ \cdots \ H_{\kappa-1}(\epsilon) \ F(\epsilon)], \quad (30)$$

where $H_i(\epsilon) \in \mathbb{R}^{m \times \ell}$ and $F(\epsilon) \in \mathbb{R}^{m \times n}$.

Finally, we note that solutions to the Riccati equation in (29) might have severe numerical problems as ϵ becomes smaller and smaller. Alternatively, one can solve the RPT control problem using a structural decomposition approach, which can be found in Chen [9].

3.2 Outer-loop control system design

As depicted in Fig. 6, the outer loop of the flight control system is for controlling the position of the unmanned rotorcraft, *i.e.*, \mathbf{P}_n . In Fig. 6, the inner-loop command generator is computed as the following:

$$\begin{pmatrix} \delta_r \\ \phi_r \\ \theta_r \end{pmatrix} = (G_{\text{in,cl},0}^{-1})\mathbf{a}_{b,r}, \quad (31)$$

where $G_{\text{in,cl},0}$ is the DC gain of the inner closed-loop system with its input variables being δ_r , ϕ_r , and θ_r and its output variables being a_x , a_y , and a_z , respectively. For HeLion with the H_∞ inner-loop controller as given in Section 2.2, the resulting DC gain is given by

$$G_{\text{in,cl},0}^{-1} = \begin{bmatrix} -0.0001 & 0.0019 & 0.0478 \\ 0.0022 & -0.1031 & -0.0048 \\ 0.1022 & 0 & 0.0002 \end{bmatrix}. \quad (32)$$

For the outer-loop control system design, we treat the closed inner-loop and the inner-loop command generator, *i.e.*, the portion inside the dashed box in Fig. 6, as a *virtual actuator* (such a design idea is illustrated in Fig. 7 for easy reference). Our design will work properly, if $\mathbf{a}_{n,r}$ with frequencies in the working range of the outer loop is able to freely pass through the virtual actuator. It indeed turns out to be the case.

Shown in Figs 8 and 9 are the frequency responses of the linearized model of the virtual actuator, which clearly indicate that all its three channels are almost perfectly decoupled. Moreover, the characteristics of both the X- and Y-channels are of low-pass systems with cutoff frequencies around 1 rad/s, whereas the Z-channel is an all-pass system. As such, it is pretty safe for us to separate the outer rotorcraft dynamics into three decoupled channels, respectively, in the X-, Y-, and Z-axes of the local NED frame, with each channel being characterized by a double integrator, provided that the actual working frequency of the outer loop is kept within the

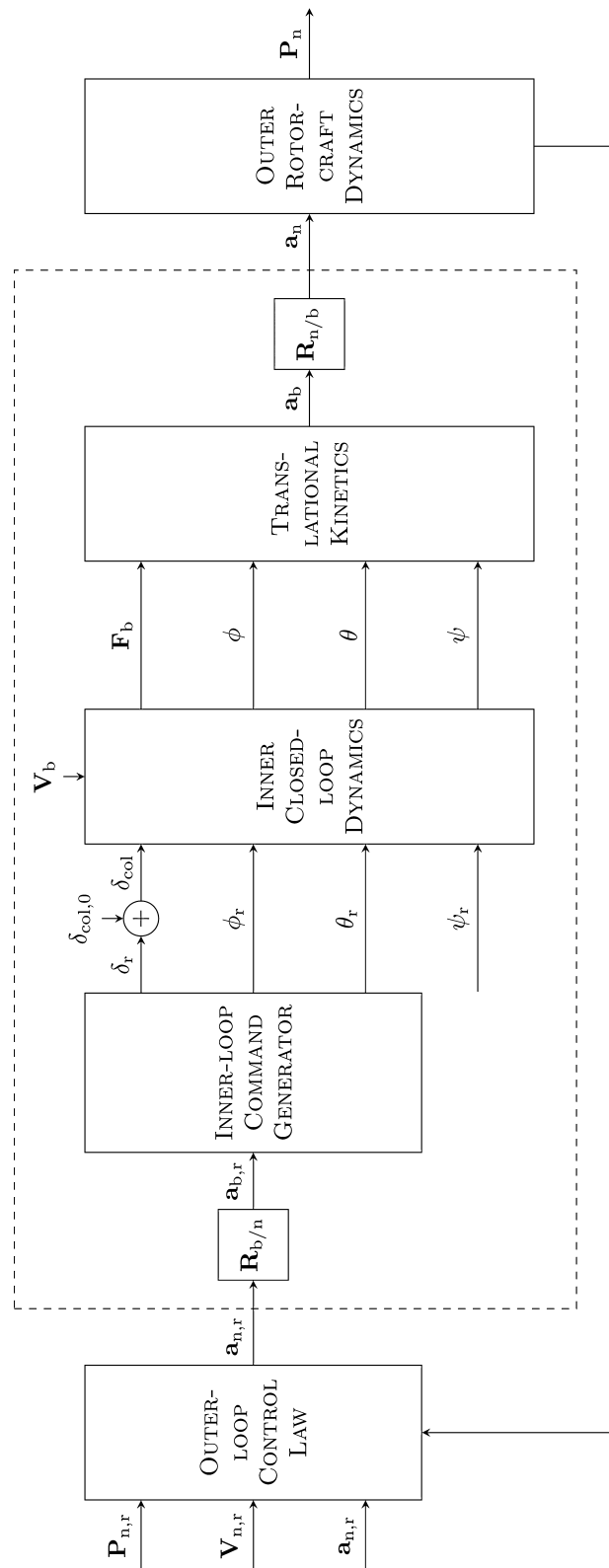


Fig. 6. Outer loop of the rotorcraft flight control system.

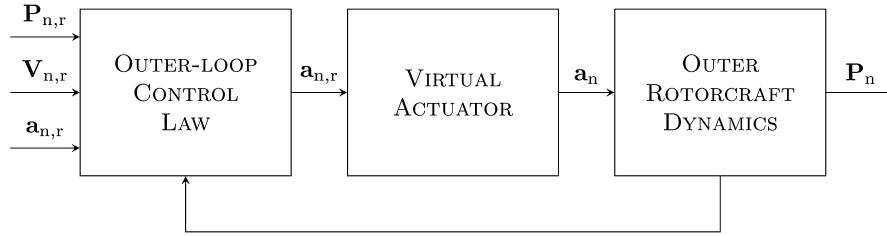


Fig. 7. Reconfiguration of the outer-loop flight control system.

bandwidth of the virtual actuator, *i.e.*, 1 rad/s. More specifically, in such a situation, the dynamical equation for the X-axis can be expressed as

$$\begin{pmatrix} \dot{x}_n \\ \dot{u}_n \end{pmatrix} = \begin{bmatrix} 0 & 1 \\ 0 & 0 \end{bmatrix} \begin{pmatrix} x_n \\ u_n \end{pmatrix} + \begin{bmatrix} 0 \\ 1 \end{bmatrix} a_{x,n}, \quad (33)$$

where x_n is the X-axis position of the UAV in the local NED frame, and u_n and $a_{x,n}$ are respectively the local NED velocity and acceleration projected onto the X-axis. Similarly, the dynamic equations for the Y- and Z-axes are given by

$$\begin{pmatrix} \dot{y}_n \\ \dot{v}_n \end{pmatrix} = \begin{bmatrix} 0 & 1 \\ 0 & 0 \end{bmatrix} \begin{pmatrix} y_n \\ v_n \end{pmatrix} + \begin{bmatrix} 0 \\ 1 \end{bmatrix} a_{y,n} \quad (34)$$

and

$$\begin{pmatrix} \dot{z}_n \\ \dot{w}_n \end{pmatrix} = \begin{bmatrix} 0 & 1 \\ 0 & 0 \end{bmatrix} \begin{pmatrix} z_n \\ w_n \end{pmatrix} + \begin{bmatrix} 0 \\ 1 \end{bmatrix} a_{z,n}, \quad (35)$$

respectively, with all of its state and control variables defined in the same fashion as those in (33). We should note that in the unmanned rotorcraft system, its position, velocity, and acceleration are all measurable and available for feedback control. It should also be noted that the disturbance we intend to reject is the wind gust. In our work, it only affects the flight dynamics via the three body-frame velocity channels. In other words, the disturbance is only considered in our inner-loop control system design. As a consequence, the outer-layer dynamics only consist of above three kinematic relationships along three NED-frame axes, without considering any disturbance effect. The disturbance term in (19), or equivalently, in (33) to (35), is thus not involved. As all three channels share the same dynamic structure, we proceed in what follows to focus on the design of the outer-loop controller for the X-axis only using the RPT control technique introduced in the previous section. The controllers for the Y-axis and the heave direction can be carried out with the same procedure.

To control the position of the UAV, we defined the controlled output associated with (33) as

$$h_x = x_n = \begin{bmatrix} 1 & 0 \end{bmatrix} \begin{pmatrix} x_n \\ u_n \end{pmatrix}. \quad (36)$$

It is straightforward to verify that the RPT control problem for the given system comprising (33) and (36) is solvable under state feedback. Since the position reference $x_{n,r}$ and its associated velocity, $u_{n,r}$, and acceleration, $a_{x,n,r}$, are all available, we formulate the problem into the RPT design framework by defining

$$\frac{d}{dt} \begin{pmatrix} x_{n,r} \\ u_{n,r} \\ a_{x,n,r} \end{pmatrix} = \begin{bmatrix} 0 & 1 & 0 \\ 0 & 0 & 1 \\ 0 & 0 & 0 \end{bmatrix} \begin{pmatrix} x_{n,r} \\ u_{n,r} \\ a_{x,n,r} \end{pmatrix} + \begin{bmatrix} 0 \\ 0 \\ 1 \end{bmatrix} \dot{a}_{x,n,r}. \quad (37)$$

We obtain an augmented system of the following form:

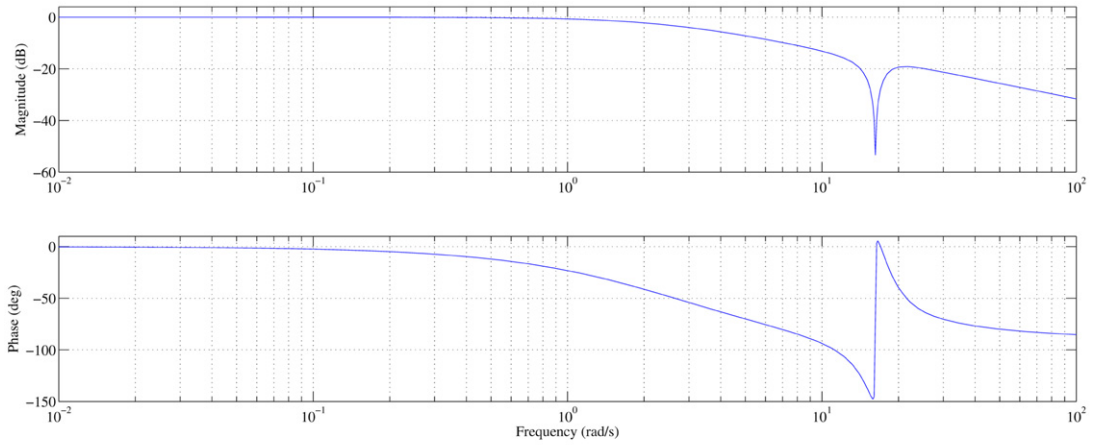
$$\Sigma_{\text{AUG}}: \begin{cases} \dot{\mathbf{x}} = \mathbf{A}\mathbf{x} + \mathbf{B}\mathbf{u} + \mathbf{E}\mathbf{w} \\ \mathbf{y} = \mathbf{x} \\ \mathbf{e} = \mathbf{C}_2\mathbf{x} \end{cases} \quad (38)$$

where

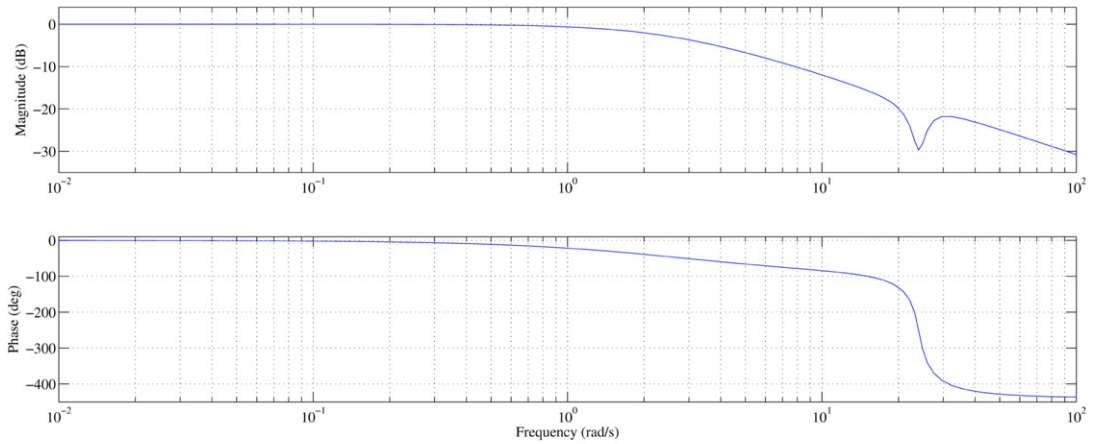
$$\mathbf{x} := \begin{pmatrix} x_{n,r} \\ u_{n,r} \\ a_{x,n,r} \\ x_n \\ u_n \end{pmatrix}, \quad \mathbf{w} := \dot{a}_{x,n,r}, \quad (39)$$

$$\mathbf{A} = \begin{bmatrix} 0 & 1 & 0 & 0 & 0 \\ 0 & 0 & 1 & 0 & 0 \\ 0 & 0 & 0 & 0 & 0 \\ 0 & 0 & 0 & 0 & 1 \\ 0 & 0 & 0 & 0 & 0 \end{bmatrix}, \quad \mathbf{B} = \begin{bmatrix} 0 \\ 0 \\ 0 \\ 0 \\ 1 \end{bmatrix}, \quad \mathbf{E} = \begin{bmatrix} 0 \\ 0 \\ 1 \\ 0 \\ 0 \end{bmatrix}, \quad (40)$$

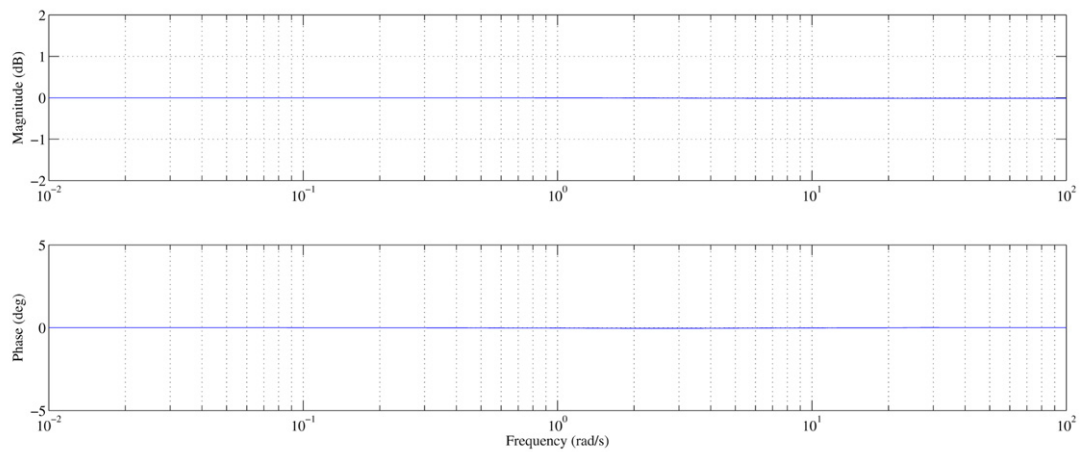
and



a. From $a_{x,n,r}$ to $a_{x,n}$

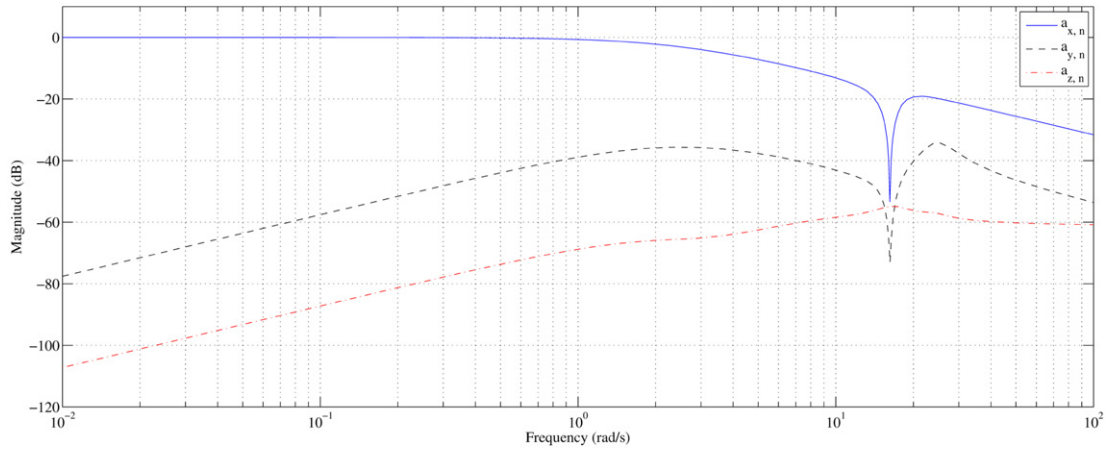


b. From $a_{y,n,r}$ to $a_{y,n}$

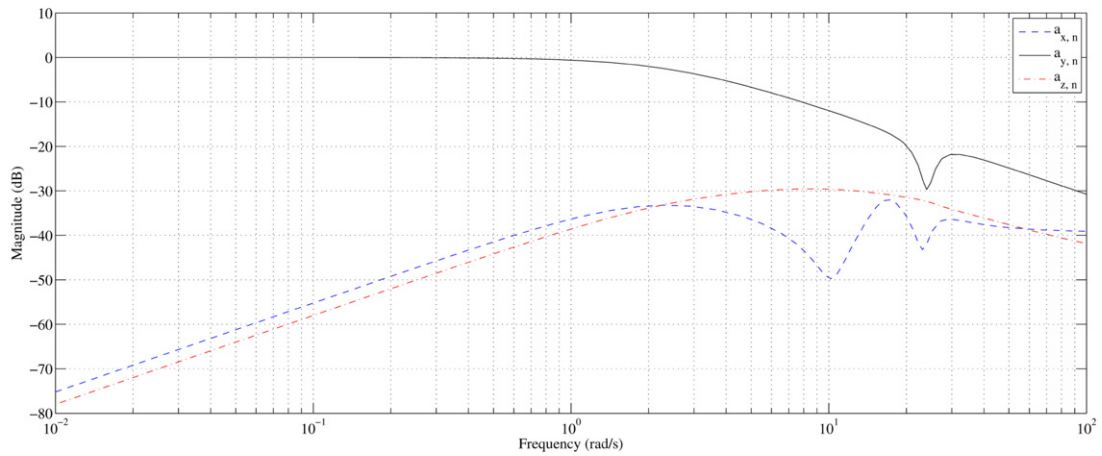


c. From $a_{z,n,r}$ to $a_{z,n}$

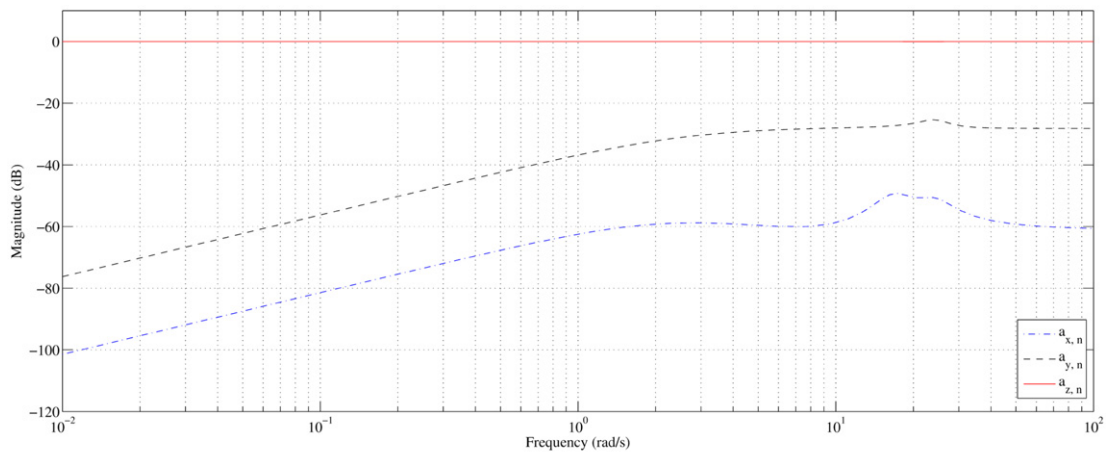
Fig. 8. Frequency responses of the main channels of the virtual actuator.



a. From $a_{x,n,r}$ to all output channels



b. From $a_{y,n,r}$ to all output channels



c. From $a_{z,n,r}$ to all output channels

Fig. 9. Magnitude responses of all channels of the virtual actuator.

$$C_2 = [-1 \ 0 \ 0 \ 1 \ 0]. \quad (41)$$

Using the procedure given in [9], we are able to obtain a closed-form solution for the state feedback gain for the system of (38) that solves the RPT control problem. The closed-form solution is given by

$$u = Fx \quad (42)$$

with

$$F = \begin{bmatrix} -\frac{\omega_{n,x}^2}{\varepsilon_x^2} & -\frac{2\zeta_x\omega_{n,x}}{\varepsilon_x} & \frac{\omega_{n,x}^2}{\varepsilon_x^2} & \frac{2\zeta_x\omega_{n,x}}{\varepsilon_x} & 1 \end{bmatrix}. \quad (43)$$

Equivalently, we have

$$\begin{aligned} a_{x,n} &= F_x(\varepsilon_x) \begin{pmatrix} x_n \\ u_n \end{pmatrix} + H_{x,0}(\varepsilon_x)x_{n,r} + H_{x,1}(\varepsilon_x)u_{n,r} \\ &\quad + H_{x,2}(\varepsilon_x)a_{x,n,r} \\ &= -\begin{bmatrix} \frac{\omega_{n,x}^2}{\varepsilon_x^2} & \frac{2\zeta_x\omega_{n,x}}{\varepsilon_x} \end{bmatrix} \begin{pmatrix} x_n \\ u_n \end{pmatrix} + \begin{pmatrix} \frac{\omega_{n,x}^2}{\varepsilon_x^2} \end{pmatrix} x_{n,r} \\ &\quad + \begin{pmatrix} \frac{2\zeta_x\omega_{n,x}}{\varepsilon_x} \end{pmatrix} u_{n,r} + a_{x,n,r}, \end{aligned} \quad (44)$$

where ε_x is the tuning parameter, and $\omega_{n,x}$ and ζ_x are respectively the nominal natural frequency and damping ratio associated with the closed-loop system of the X-axis dynamics. More specifically, the closed-loop eigenvalues of the X-axis dynamical system under the state feedback control are given by

$$-\frac{\zeta_x\omega_{n,x}}{\varepsilon_x} \pm j\frac{\omega_{n,x}\sqrt{1-\zeta_x^2}}{\varepsilon_x}. \quad (45)$$

Similarly, following the same procedure, we can obtain the controllers for the Y-axis dynamics and the heave dynamics respectively as

$$\begin{aligned} a_{y,n} &= -\begin{bmatrix} \frac{\omega_{n,y}^2}{\varepsilon_y^2} & \frac{2\zeta_y\omega_{n,y}}{\varepsilon_y} \end{bmatrix} \begin{pmatrix} y_n \\ v_n \end{pmatrix} + \begin{pmatrix} \frac{\omega_{n,y}^2}{\varepsilon_y^2} \end{pmatrix} y_{n,r} \\ &\quad + \begin{pmatrix} \frac{2\zeta_y\omega_{n,y}}{\varepsilon_y} \end{pmatrix} v_{n,r} + a_{y,n,r} \end{aligned} \quad (46)$$

and

$$\begin{aligned} a_{z,n} &= -\begin{bmatrix} \frac{\omega_{n,z}^2}{\varepsilon_z^2} & \frac{2\zeta_z\omega_{n,z}}{\varepsilon_z} \end{bmatrix} \begin{pmatrix} z_n \\ w_n \end{pmatrix} + \begin{pmatrix} \frac{\omega_{n,z}^2}{\varepsilon_z^2} \end{pmatrix} z_{n,r} \\ &\quad + \begin{pmatrix} \frac{2\zeta_z\omega_{n,z}}{\varepsilon_z} \end{pmatrix} w_{n,r} + a_{z,n,r}. \end{aligned} \quad (47)$$

In principle, the RPT controllers above are capable of achieving an arbitrarily fast response if the tuning parameters are chosen to be sufficiently small. However, we need to follow several design specifications to account for both the

physical feature of miniature rotorcraft and the feasibility of practical implementations. More specifically:

1. The response of the outer-loop system is required to be slower than the bandwidth of the virtual actuator, *i.e.*, 1 rad/s.
2. To minimize overshoots in time-domain responses, the damping ratios for all these three channels should be selected to be greater than or equal to unity.
3. The closed outer-loop dynamics should have sufficient gain and phase margins.

Based on these guidelines, we finally select the following outer-loop controller parameters for HeLion:

$$\omega_{n,x} = 0.54, \quad \omega_{n,y} = 0.62, \quad \omega_{n,z} = 0.78, \quad (48)$$

$$\varepsilon_x = \varepsilon_y = \varepsilon_z = 1, \quad (49)$$

and

$$\zeta_x = 1, \quad \zeta_y = 1, \quad \zeta_z = 1.1. \quad (50)$$

We note that in order to minimize overshoots in time-domain responses, the damping ratios for all three channels are selected to be greater than or equal to unity.

In order to verify the robustness of the outer-loop flight control system, we examine the frequency response of each individual channel of the outer-loop system, which are respectively shown in Figs 10 to 12. It is clear that all the channels have an infinite gain margin and a phase margin greater than 75 degrees. The overall outer-loop system is robust enough to handle the external disturbances and uncertainties resulting from the *virtual actuator* of the inner-loop layer.

IV. SIMULATION AND IMPLEMENTATION RESULTS

Before conducting actual flight tests, we have carried out a series of hardware-in-the-loop simulations to evaluate effectively the reliability and performance of HeLion. In our proposed hardware-in-the-loop simulation framework detailed in [7], the key components of the unmanned system, including the RC helicopter, the avionic system, and the ground control station, are activated to maximally emulate HeLion maneuvering in real flight. As a result, any harmful deficiencies or improper designs can be discovered and the probability of flight accidents can then be minimized. In the hardware-in-the-loop simulations, we mainly intend to evaluate the wind gust disturbance attenuation, and the tracking performance of position and velocity. More specifically, Figs 13 to 15 show the position and velocity hold performance with the overall system due to a wind gust,

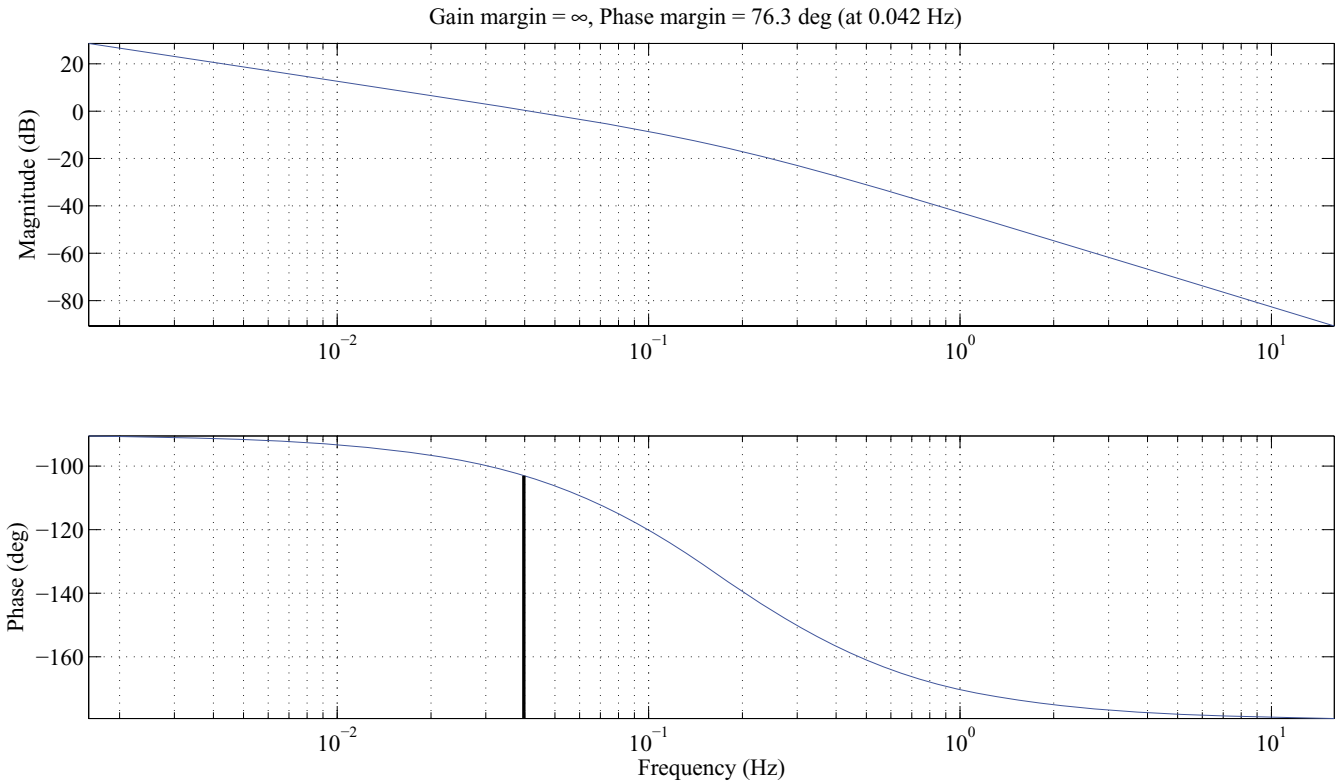


Fig. 10. Gain and phase margins of local NED X-axis position control.

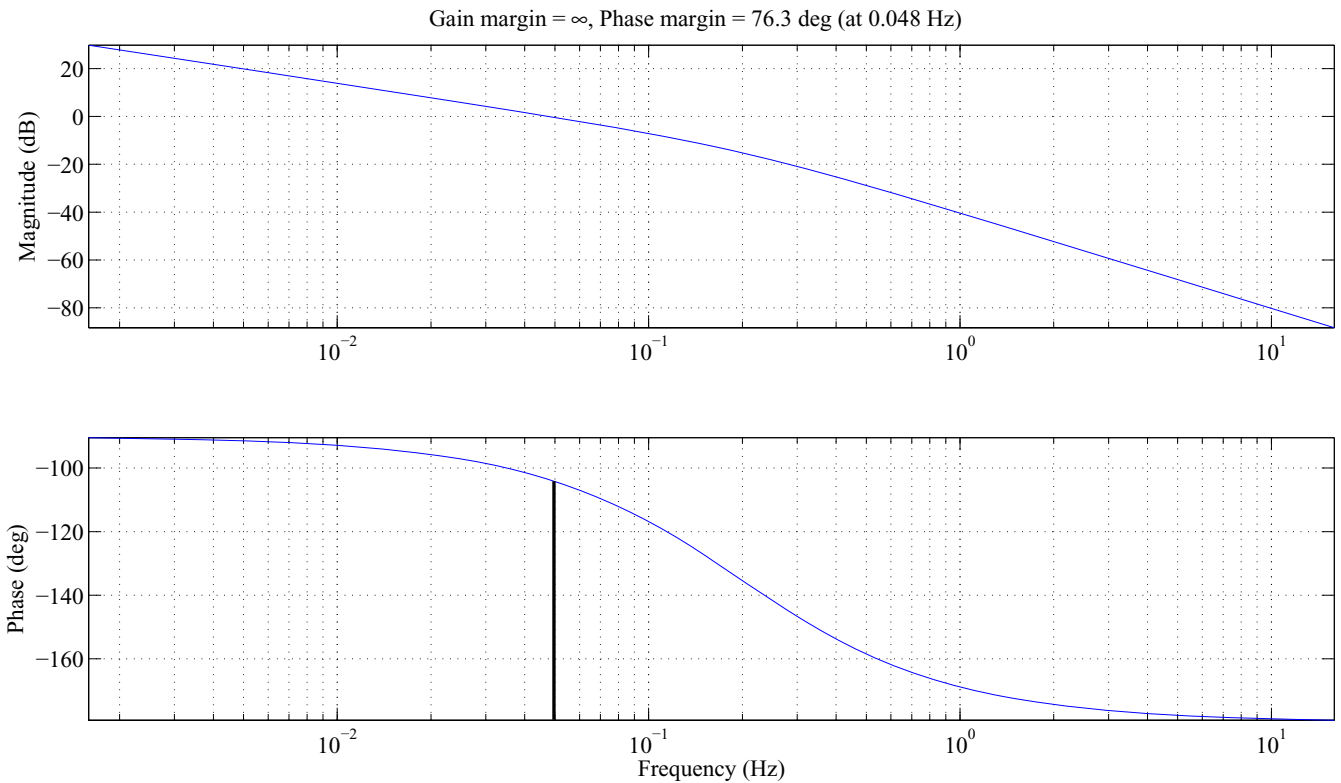


Fig. 11. Gain and phase margins of local NED Y-axis position control.

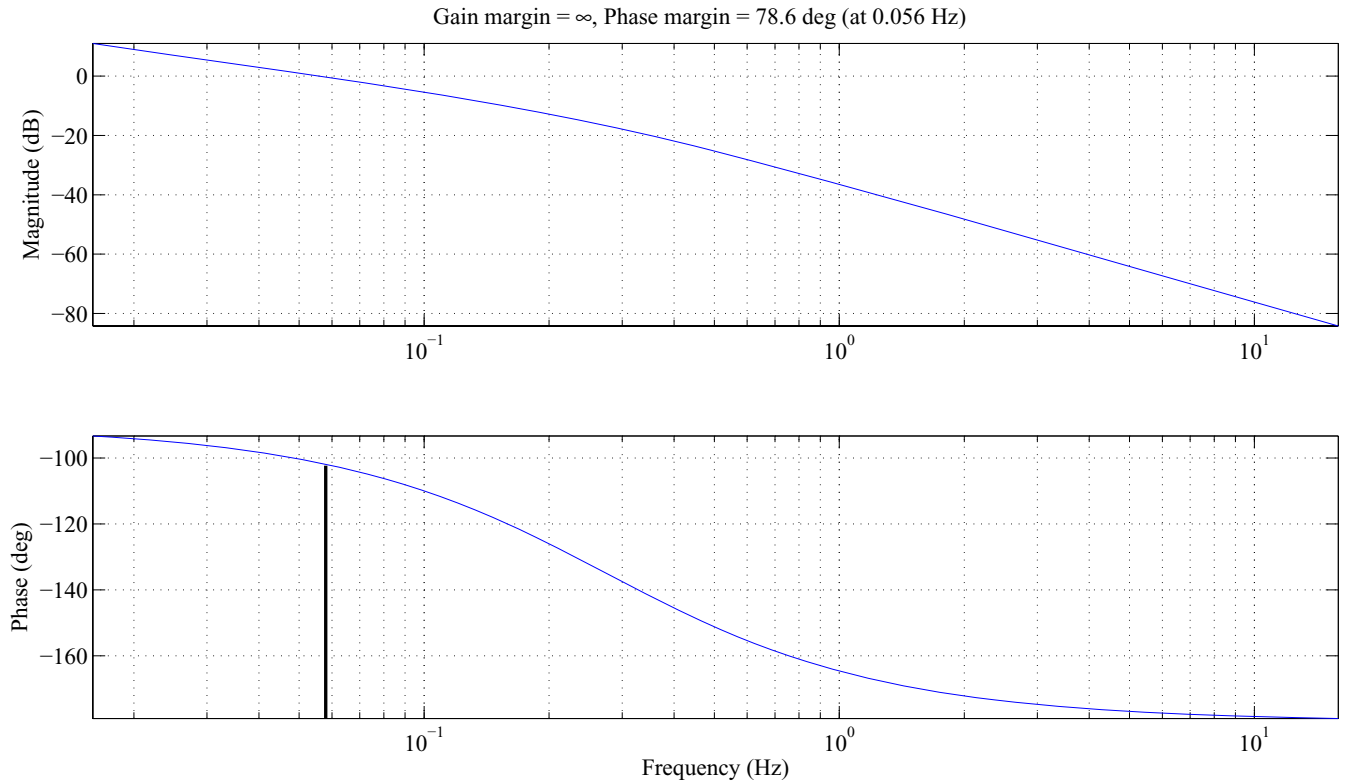


Fig. 12. Gain and phase margins of local NED Z-axis position control.

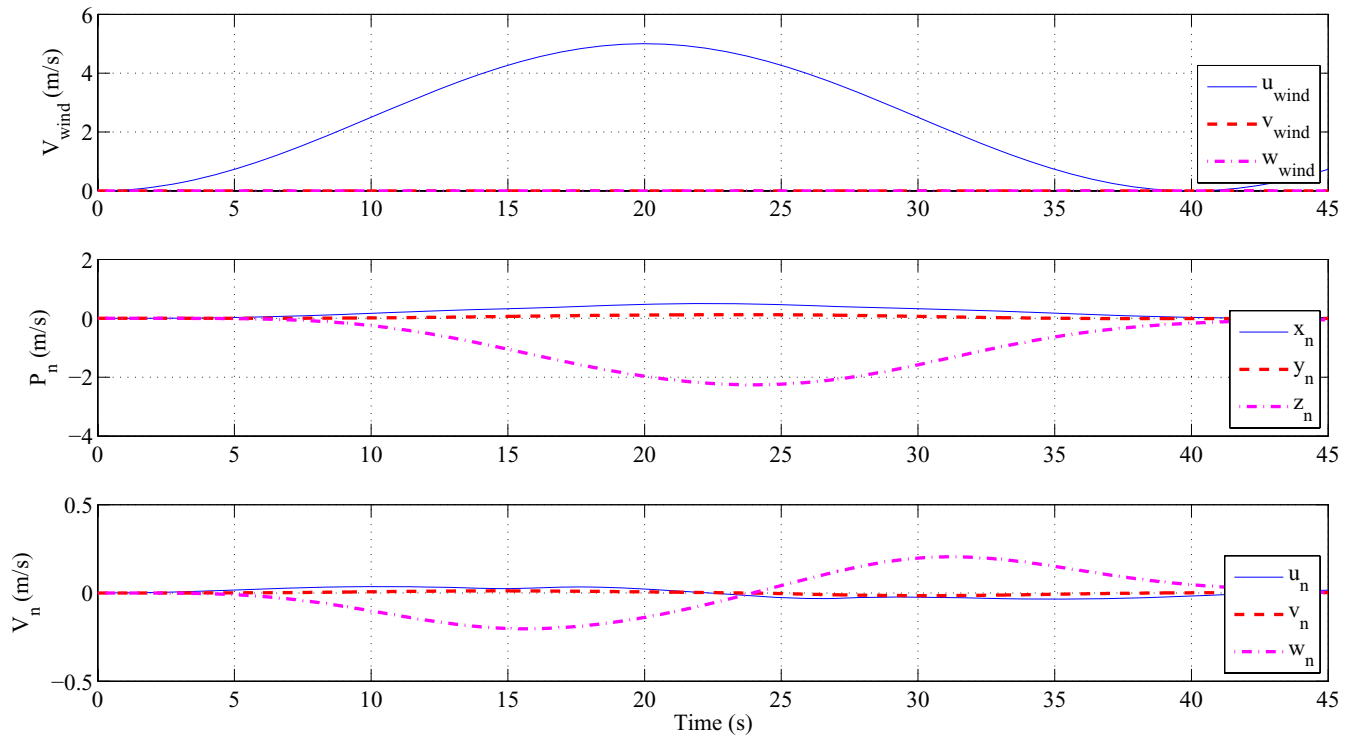


Fig. 13. Wind gust disturbance attenuation along local-NED X-axis direction.

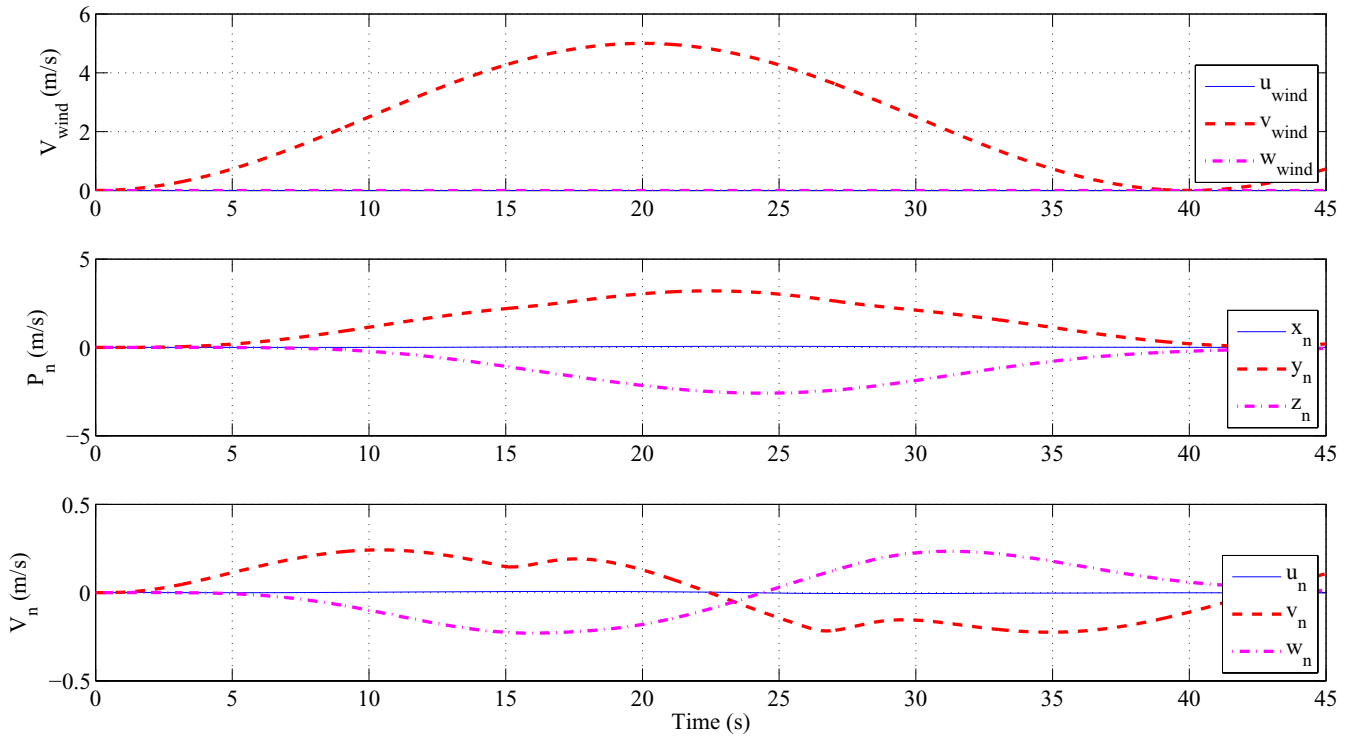


Fig. 14. Wind gust disturbance attenuation along local-NED Y-axis direction.

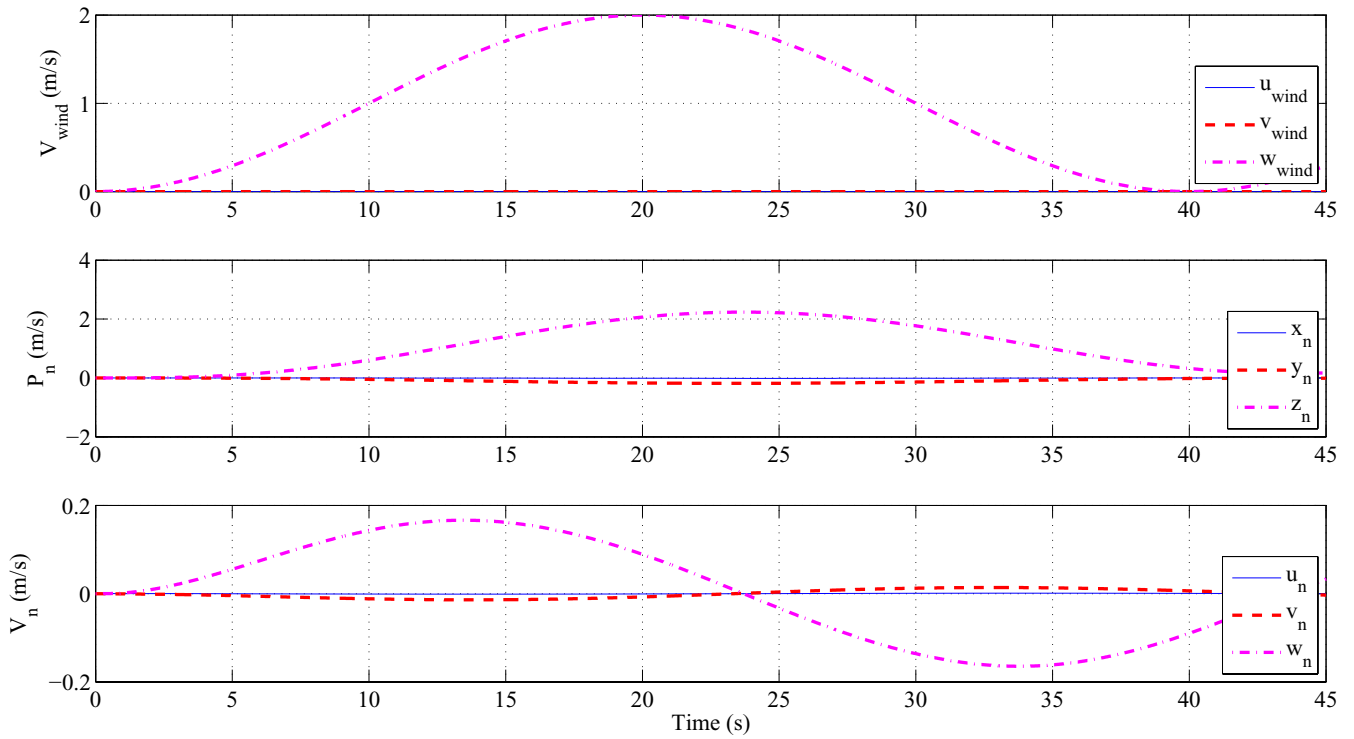


Fig. 15. Wind gust disturbance attenuation along local-NED Z-axis direction.

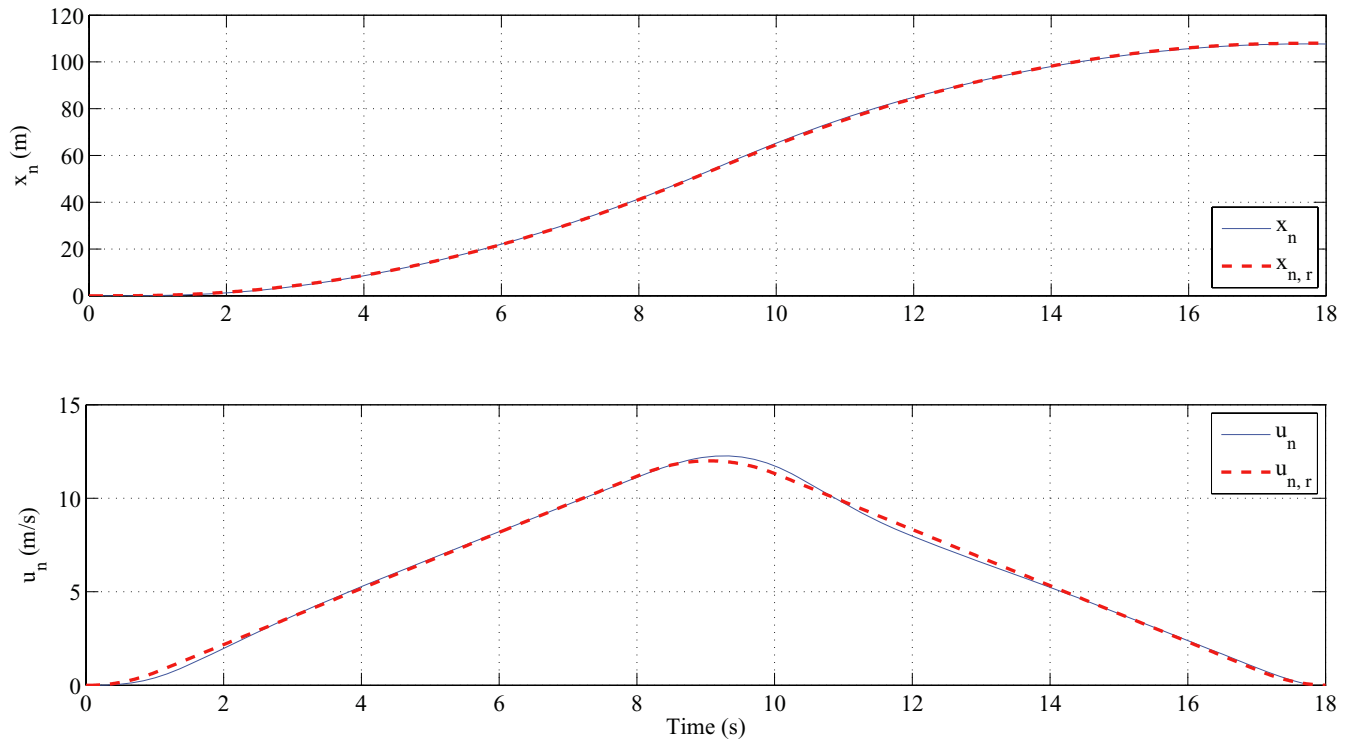


Fig. 16. Tracking performance evaluation along local NED X-axis direction.

whereas Figs 16 to 18 demonstrate the evaluation results of tracking performance. It is noted that for tracking performance we examine three flight motions. In the first maneuver, HeLion starts with a stable hover with heading to the north direction, then conducts a forward acceleration to 12 m/s, and finally decelerates to another stable hover. The other two maneuvers are similar to the first one, but with the acceleration/deceleration directions being changed to the east and upward and with the top sideslip and heave speed being 6 m/s and 2.5 m/s, respectively. It is clear that the overall performance is very satisfactory in simulation. Then more completed tests on the actual flight implementation can be conducted.

Next, we present the results of the actual flight test experiments to evaluate the performance of the outer-loop control system using RPT technique. To realize this aim, a series of mission-task-elements (MTEs), which are originally set in ADS-33D-PRF [2] for evaluating military rotorcraft' performance, have been adopted. More specifically, nine MTEs, including: (i) depart/abort (forward flight); (ii) hover; (iii) depart/abort (backward flight); (iv) hovering turn; (v) vertical maneuver; (vi) lateral reposition; (vii) turn-to-target; (viii) slalom; and (ix) pirouette, have been selected. These MTEs are then concatenated sequentially to form an appropriate flight trajectory for the outmost layer, *i.e.*, the flight scheduling layer, in our proposed flight

control structure (see Fig. 1). The recorded position and velocity responses are shown from Figs 19 and 20. We need to highlight that:

1. All the nine MTEs have been fully completed in automatic control mode.
2. During the flight test, the horizontal wind gust is about 4 m/s, which is roughly recorded by handheld anemometer. With this disturbance, the predefined flight trajectory can still be well maintained.
3. According to the specific requirements on MTEs given in [2], our RPT-based flight control system can achieve the top-level performance in terms of position and velocity tracking for each selected MTE. In Tables II and III together with Figs 21 and 22, we present the evaluation results of two specific cases with the moderate aggressiveness (*i.e.*, depart/abort, forward flight, and slalom) for illustration.
4. We have noticed that there are minor gaps between the flight responses and the simulation results. In terms of position and velocity, the small differences have the amplitudes of only 2 m and 1 m/s, respectively. Such inconsistencies are caused by the combination of a series of factors, including: (i) the slightly remnant wind gust disturbance which cannot be completely rejected by the inner-loop control system; (ii) the minor

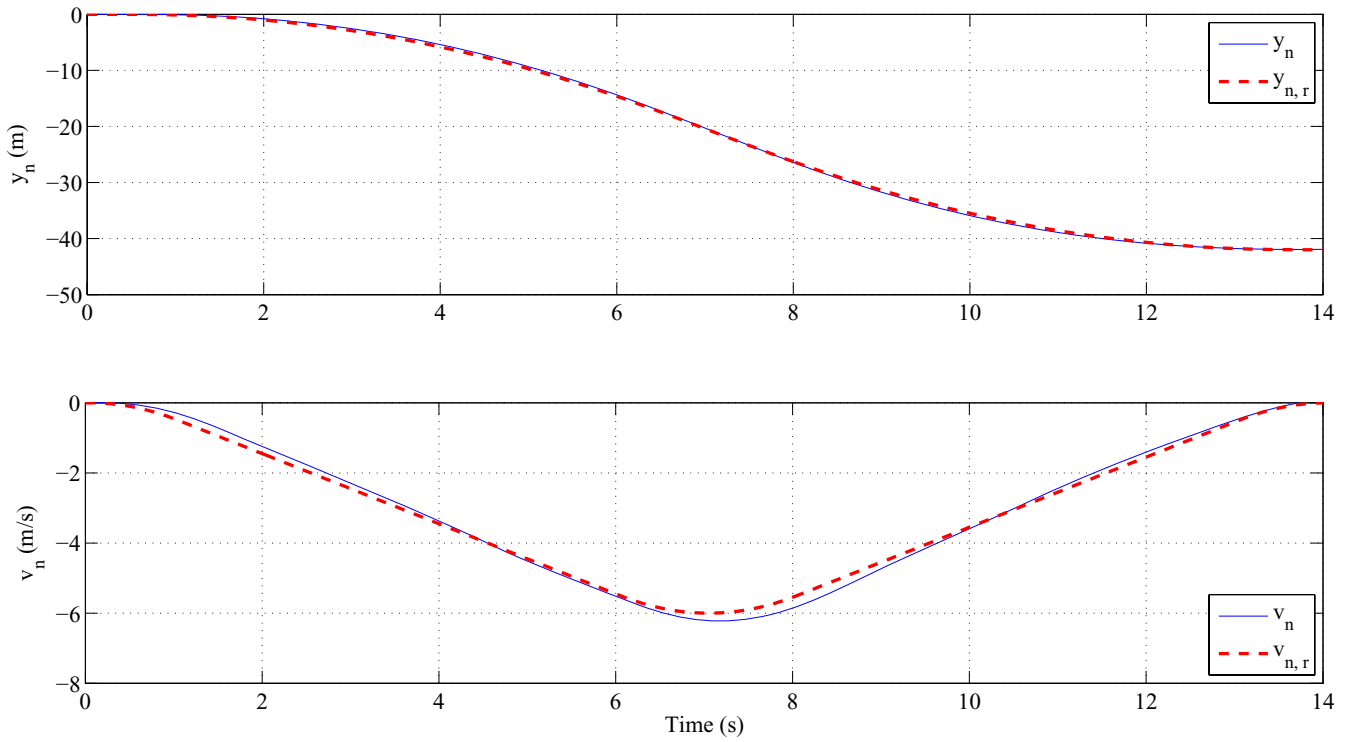


Fig. 17. Tracking performance evaluation along local NED Y-axis direction.

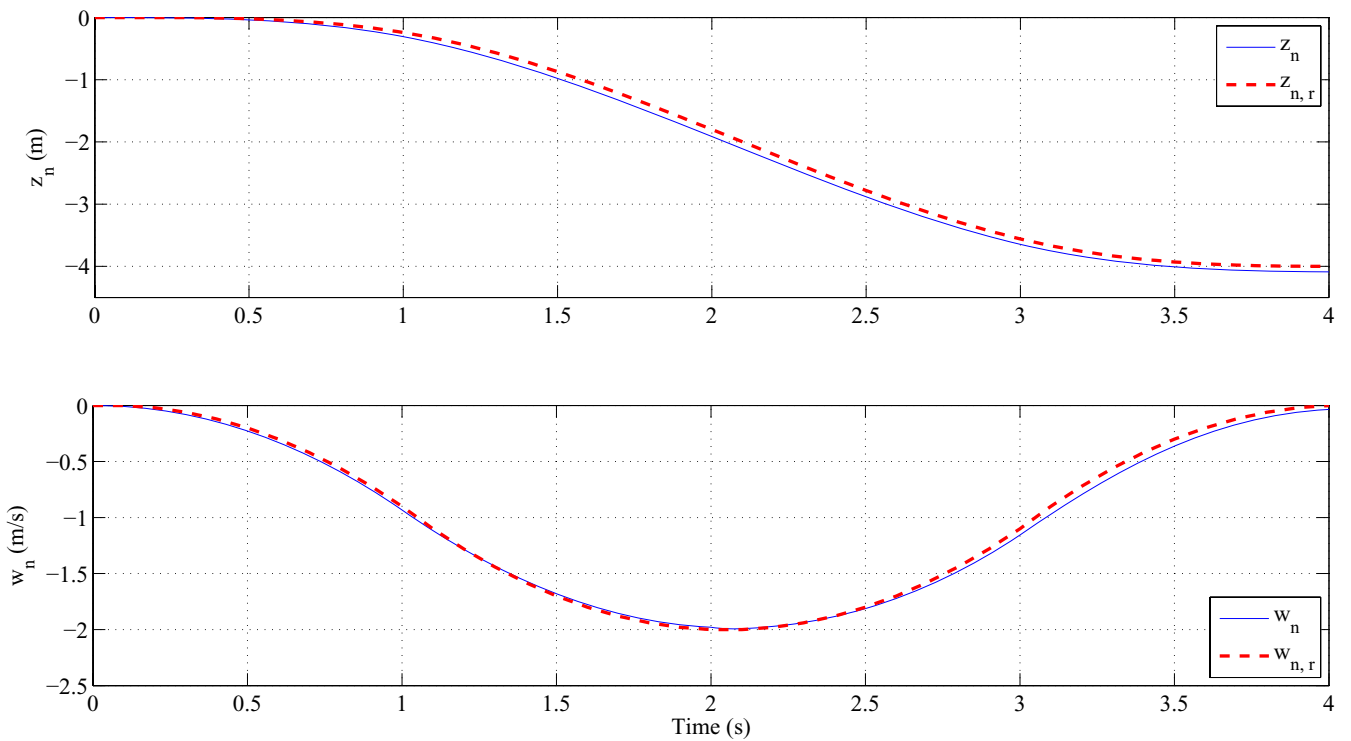


Fig. 18. Tracking performance evaluation along local NED Z-axis direction.

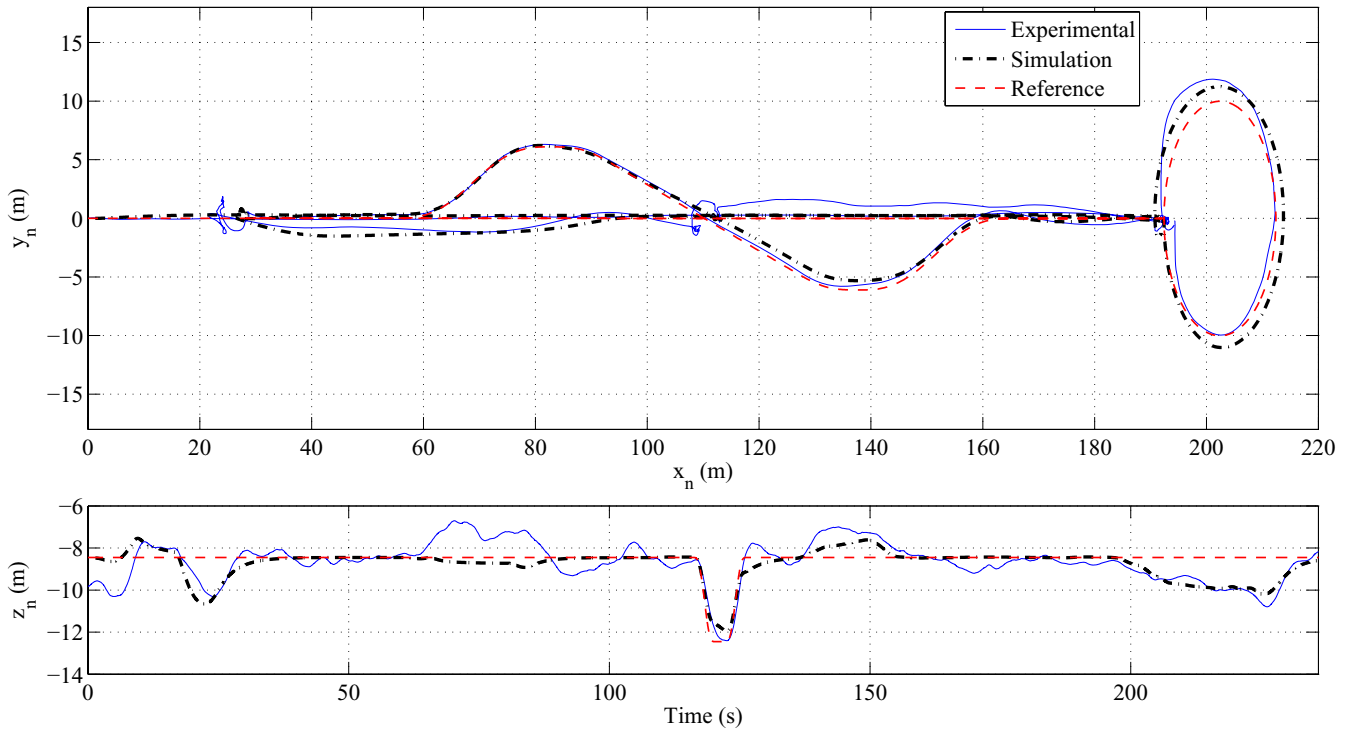


Fig. 19. Position responses of the wide-envelope flight.

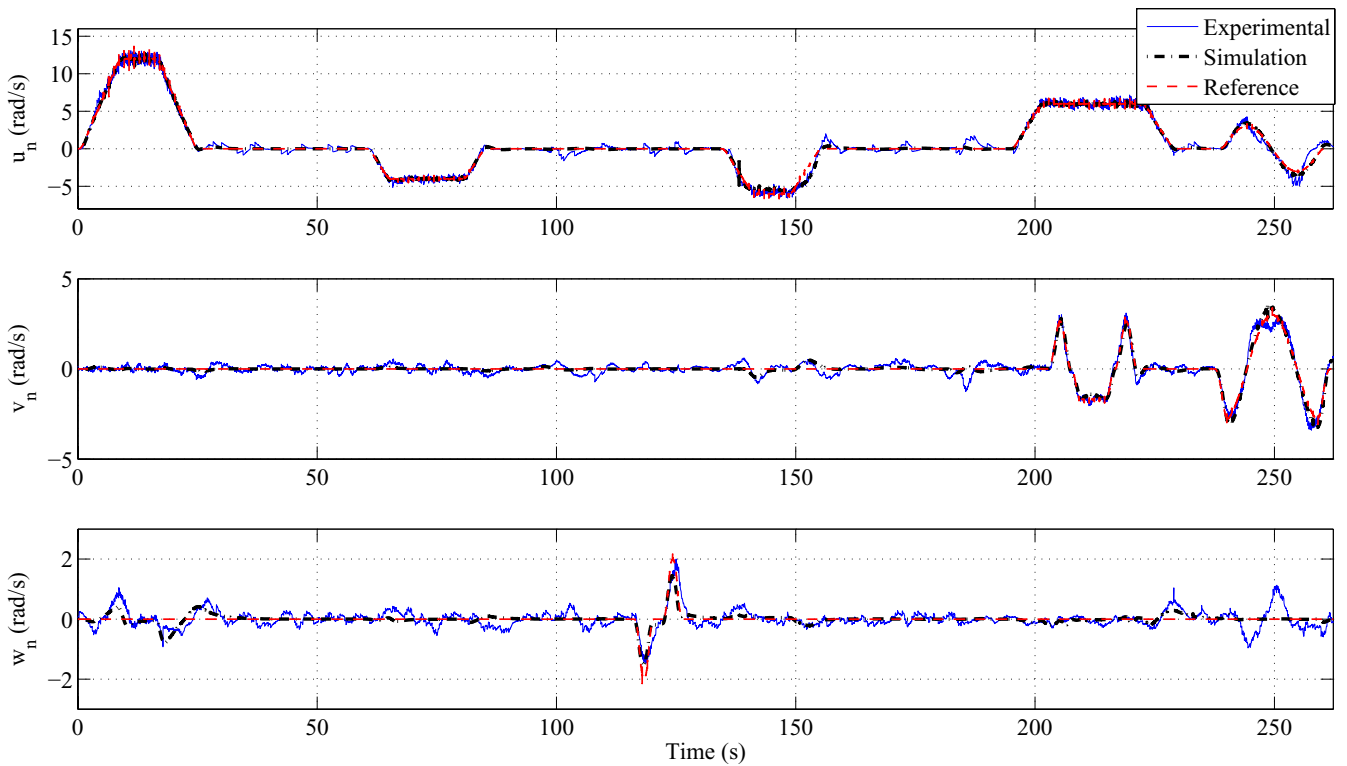
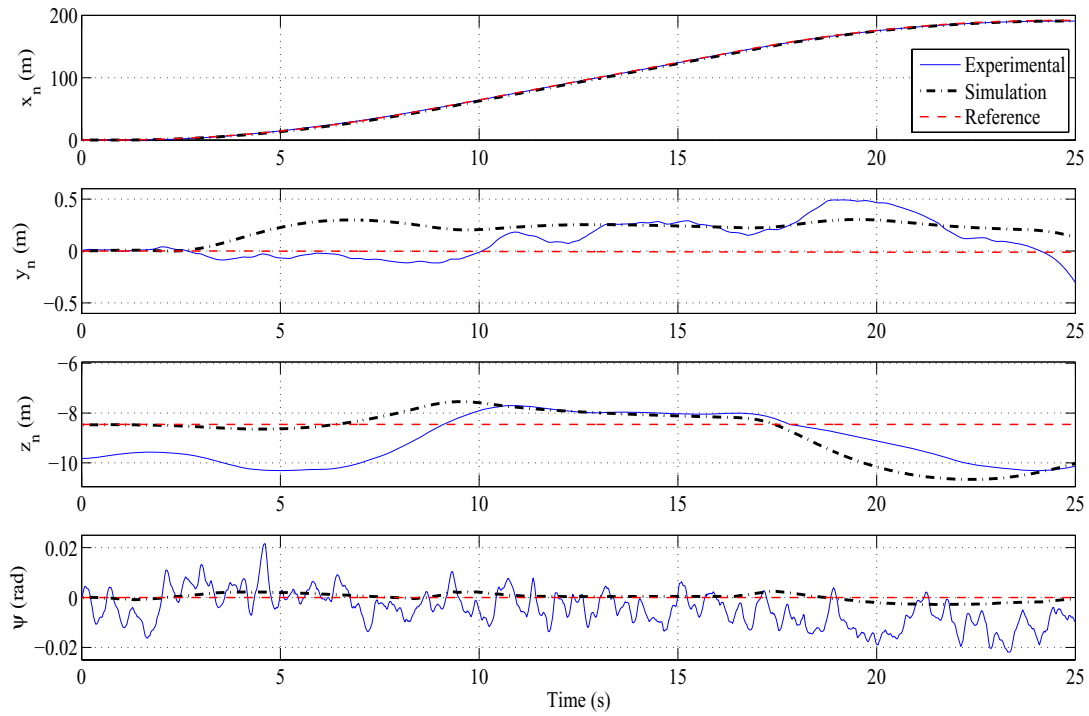
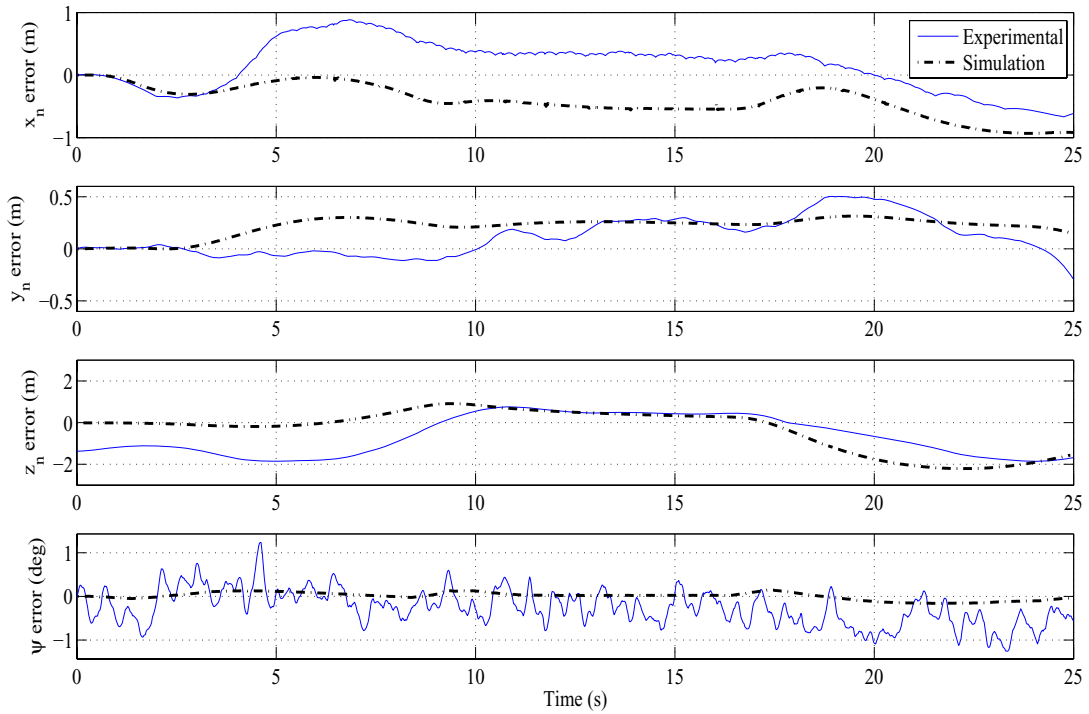


Fig. 20. Velocity responses of the wide-envelope flight.

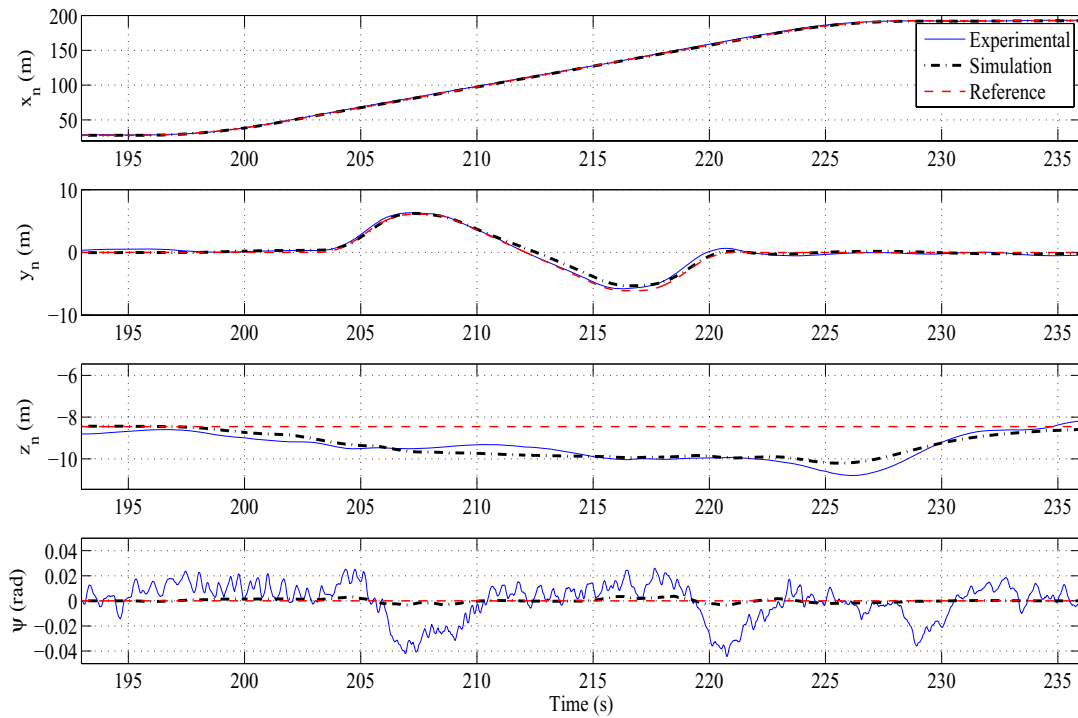


a. Simulation and experimental responses of depart/abort forward flight

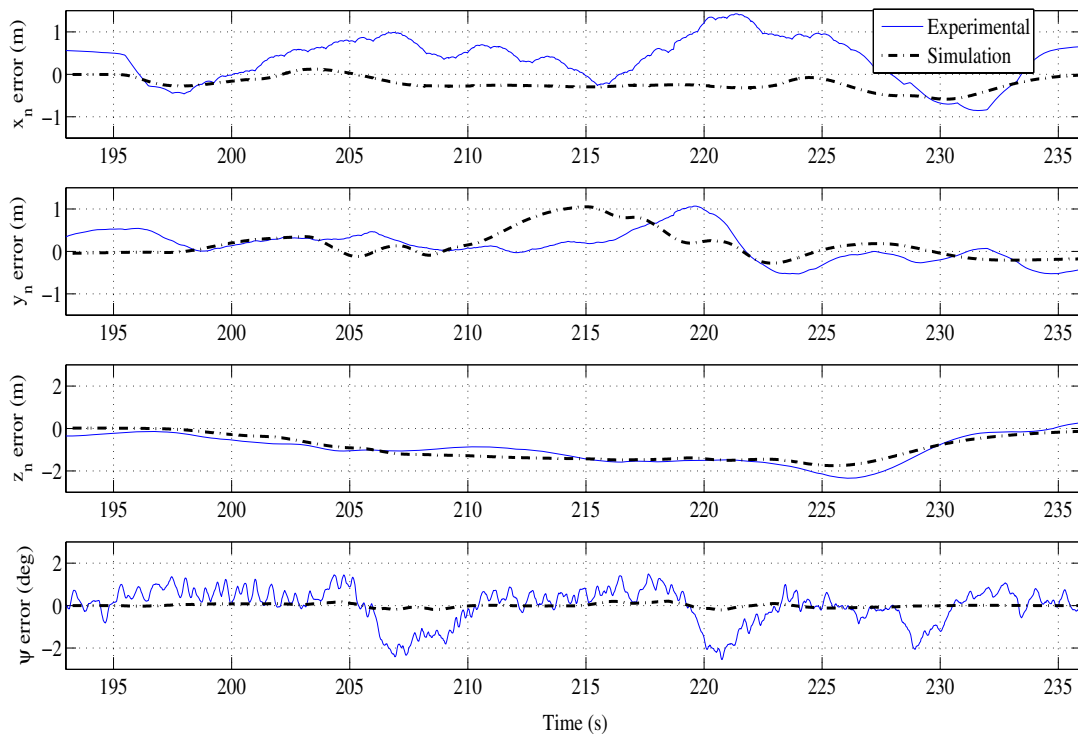


b. Tracking errors of depart/abort forward flight

Fig. 21. Depart/abort forward flight result.



a. Simulation and experimental responses of slalom



b. Tracking errors of slalom

Fig. 22. Slalom flight result.

Table II. Depart/abort (forward flight) performance evaluation.

| Specifications | Desired level | Simulation | Actual test |
|-------------------------------|-----------------|-------------------|-------------------|
| Longitudinal position error | ≤ 3 m | ≤ 0.93 m | ≤ 0.88 m |
| Lateral position error | ≤ 3 m | ≤ 0.31 m | ≤ 0.51 m |
| Altitude error | ≤ 3 m | ≤ 2.16 m | ≤ 1.85 m |
| Heading error | $\leq 10^\circ$ | $\leq 0.14^\circ$ | $\leq 1.24^\circ$ |
| Time to complete the maneuver | ≤ 25 s | 25 s | 25 s |

Table III. Slalom performance evaluation.

| Specifications | Desired level | Simulation | Actual test |
|-----------------------------|-----------------|-------------------|-------------------|
| Maintaining forward speed | ≥ 6 m/s | 6 m/s | 6 m/s |
| Longitudinal position error | ≤ 2 m | ≤ 0.56 m | ≤ 1.41 m |
| Lateral position error | ≤ 2 m | ≤ 1.05 m | ≤ 1.06 m |
| Altitude error | ≤ 3 m | ≤ 1.73 m | ≤ 2.33 m |
| Heading error | $\leq 10^\circ$ | $\leq 0.18^\circ$ | $\leq 2.54^\circ$ |

but unavoidable uncertainty of the flight dynamics model; and (iii) other minor environmental disturbances in the flight experiments.

The results obtained clearly indicate that our control system design using the RPT technique is very successful. The unmanned rotorcraft system is capable of achieving the desired performance in accordance with the military standard under examination. Interested readers can access the video clips of the actual flight tests on our UAV research group website at <http://uav.ece.nus.edu.sg>.

V. CONCLUSION

We have presented in this paper a flight control system design, more specifically, the design of the outer-loop layer of the flight control system, using the robust and perfect tracking control technique. The simulation and actual implementation results have shown that the overall design is very satisfactory and is capable of achieving the top level performance in accordance with the standards set for military rotorcraft by US Army Aviation [2]. The unique feature of the RPT control can also be adopted for realizing the flight formation of multiple aerial vehicles.

REFERENCES

1. Abbeel, P., A. Coates, and A. Y. Ng, "Autonomous Helicopter Aerobatics through Apprenticeship Learning," *Int. J. Robot. Res.*, Vol. 29, No. 13, pp. 1608–1631 (2010).

2. ADS-33D-PRF, *Aeronautical design standard performance specification handling qualities requirements for military rotorcraft*, U.S. Army Aviation and Troop Command, Redstone Arsenal, Alabama (1996).
3. Bogdanov, A. and E. Wan, "SDRE control with nonlinear feed forward compensation for a small unmanned helicopter," *Proc. 2nd AIAA Unmanned Unlimited Syst., Technol., Oper. Conf.*, San Diego, CA, AIAA-2003-6512 (2003).
4. Cai, G., B. M. Chen, and T. H. Lee, "Design and implementation of robust automatic flight control system for a small-scale UAV helicopter," *Proc. 7th Asian Control. Conf.*, Hong Kong, China, pp. 691–697 (2009).
5. Cai, G., B. M. Chen, and T. H. Lee, *Unmanned Rotorcraft Systems*, Springer, New York, NY, (2011).
6. Cai, G., F. Lin, B. M. Chen, and T.H. Lee, "Systematic design methodology and construction of UAV helicopters," *Mechatronics*, Vol. 18, No. 10, pp. 545–558 (2008).
7. Cai, G., B. M. Chen, T. H. Lee, and M. Dong, "Design and implementation of a hardware-in-the-loop simulation system for small-scale UAV helicopters," *Mechatronics*, Vol. 19, No. 7, pp. 1057–1066 (2009).
8. Cai, G., B. M. Chen, T. H. Lee, and K. Y. Lum, "Comprehensive nonlinear modeling of an unmanned aerial vehicle helicopter," *Proc. 2008 AIAA Guidance, Navigation and Control Conf.*, Honolulu, HI, AIAA-2008-7414 (2008).
9. Chen, B. M., *Robust and H_∞ Control*, Springer, New York, NY, (2000).
10. Chen, B. M., Z. Lin, and K. Liu, "Robust and perfect tracking of discrete-time systems," *Automatica*, Vol. 38, No. 2, pp. 293–299 (2002).
11. Corban, J. E., A. J. Calise, and J. V. R. Prasad, "Implementation of adaptive nonlinear controller for flight test on an unmanned helicopter," *Proc. 37th IEEE Conf. Dec. Control*, Tampa, FL, pp. 3641–3646 (1998).
12. Draganflyer X4 quadrotor helicopter, <http://www.draganfly.com/> (2011).
13. Efe, M. O., "Battery power loss compensated fractional order sliding mode control of a quadrotor UAV," *Asian J. Control*, doi: 10.1002/asjc.340 (2012).
14. Enns, R. and J. Si, "Helicopter flight control design using a learning control approach," *Proc. 39th IEEE Conf. Dec. Control*, Sydney, Australia, pp. 1754–1759 (2000).
15. Enns, R. and J. Si, "Helicopter trimming and tracking control using direct neural dynamic programming," *IEEE Trans. Neural Netw.*, Vol. 14, No. 4, pp. 929–939 (2003).
16. Fujiwara, D., J. Shin, K. Hazawa, and K. Nonami, " H_∞ hovering and guidance control for autonomous small-scale unmanned helicopter," *Proc. IEEE/RSJ Int. Conf. Intell Robot. Syst.*, Sendai, Japan, pp. 2463–2468 (2004).

17. Gadewadikar, J., F. L. Lewis, K. Subbarao, and B. M. Chen, "Structured H_8 command and control loop design for unmanned helicopters," *AIAA J. Guid., Control Dyn.*, Vol. 31, No. 4, pp. 1093–1102 (2008).
18. Heffley, R. K. and M. A. Mnich, *Minimum-complexity Helicopter Simulation Math Model*, Technical Report NASA Contractor Report 177476, NASA (1988).
19. Isidori, A., L. Marconi, and A. Serrani, "Robust nonlinear motion control of a helicopter," *IEEE Trans. Autom. Control*, Vol. 48, No. 3, pp. 413–426 (2003).
20. Kadmiry, B., *Fuzzy Control for an Autonomous Helicopter*, M.Sc. Thesis, Linkoping University, Sweden (2002).
21. Koo, T. J. and S. Sastry, "Output tracking control design of a helicopter model based on approximate linearization," *Proc. 37th IEEE Conf. Dec. Control*, Tampa, FL, pp. 3635–3640 (1998).
22. Lee, C.-T. and C.-C. Tsai, "Adaptive backstepping integral control of a small-scale helicopter for airdrop missions," *Asian J. Control*, Vol. 12, No. 4, pp. 531–541 (2010).
23. Mellinger, D., N. Michael, and V. Kumar, "Trajectory generation and control for precise aggressive maneuvers with quadrotors," *Int. Symposium on Experimental Robotics*, New Delhi, India (2010).
24. Mettler, B. M., *Identification, Modeling and Characteristics of Miniature Rotorcraft*, Kluwer Academic Publishers, Boston, MA, (2002).
25. Peng, K., G. Cai, B. M. Chen, M. Dong, K. Y. Lum, and T. H. Lee, "Design and implementation of an autonomous flight control law for a UAV helicopter," *Automatica* Vol. 45, No. 10, pp. 2333–2338 (2009).
26. Shakernia, O., Y. Ma, T. J. Koo, and S. Sastry, "Landing an unmanned air vehicle: vision based motion estimation and nonlinear control," *Asian J. Control*, Vol. 1, No. 3, pp. 128–145 (1999).
27. Shim, D. H., H. J. Kim, and S. Sastry, "Control system design for rotorcraft-based unmanned aerial vehicle using time-domain system identification," *Proc. IEEE Conf. Control Appl.*, Anchorage, AK, pp. 808–813 (2000).
28. Shim, D. H., H. J. Kim, and S. Sastry, "Decentralized nonlinear model predictive control of multiple flying robots," *Proc. 42nd IEEE Conf. Dec. Control*, Maui, HI, pp. 3621–3626 (2003).
29. Sky Surveyor UAV helicopters, <http://me2.tm.chiba-u.jp/uav/main/> (2011).
30. Stevens, B. L. and F. L. Lewis, *Aircraft Control and Simulation*, 2nd ed. John Wiley, Hoboken, NJ, (2003).
31. Sugeno, M., I. Hirano, S. Nakamura, and S. Kotsu, "Development of an intelligent unmanned helicopter," *Proc. 1995 IEEE Int. Conf. Fuzzy Syst.*, Yokohama, Japan, pp. 33–34 (1995).
32. Wan, E. A. and A. A. Bogdanov, "Model predictive neural control with applications to a 6 DoF helicopter model," *Proc. 2001 Amer. Control Conf.*, Arlington, VA, pp. 488–493 (2001).
33. Weilenmann, M. W., U. Christen, and H. P. Geering, "Robust helicopter position control at hover," *Proc. Amer. Control Conf.*, Baltimore, MD, pp. 2491–2495 (1994).
34. Weilenmann, M. W. and H. P. Geering, "Test bench for rotorcraft hover control," *J. Guid., Control Dyn.* Vol. 17, No. 4, pp. 729–736 (1994).



Guowei Cai received his B.E. degree in Electrical and Electronics Engineering from Tianjin University, Tianjin, China, in 2002, and his Ph.D. degree in Electrical and Computer Engineering from National University of Singapore, Singapore, in 2009. From 2008 to 2009, he was a research fellow in Department of Electrical and Computer Engineering, National University of Singapore, Singapore. Since 2009, he has been a research scientist in Temasek Laboratories, National University of Singapore. His research focuses are miniature fixed-wing or rotorcraft unmanned aerial systems. He was a recipient of the Best Application Paper Prize at the 7th Asian Control Conference, Hong Kong, China (2009).



Biao Wang received his Bachelor degree in Aero-engine Control, Master degree in Aero Engines, and Ph.D. degree in Guidance, Navigation and Control, all from Nanjing University of Aeronautics and Astronautics, China, in 1997, 2000, and 2004, respectively. He is currently Associate Professor in Department of Automatic Control, Nanjing University of Aeronautics and Astronautics, and a visiting research fellow in Department of Electrical and Computer Engineering, National University of Singapore.

Dr Wang's current research interests are in the areas of linear systems, robust and optimal control, flight control and simulation, computer vision, and unmanned aerial vehicles.



Ben M. Chen received his B.S. degree in Mathematics and Computer Science from Xiamen University, China, in 1983, M.S. degree in Electrical Engineering from Gonzaga University, USA, in 1988, and Ph.D. degree in Electrical and Computer Engineering from Washington State University, USA, in 1991. He was a software engineer in South-China Computer Corporation, Guangzhou, China, from 1983 to 1986, and was Assistant Professor from 1992 to 1993 in Department of Electrical Engineering, State University of

New York at Stony Brook, USA. Since August 1993, he has been with Department of Electrical and Computer Engineering, National University of Singapore, where he is currently a Professor. His current research interests are in robust control, systems theory, unmanned systems and financial market modeling.

He is the author/co-author of 8 research monographs including *H₂ Optimal Control* (London: Prentice Hall, 1995); *H_∞ Control and Its Applications* (New York: Springer, 1998, Chinese edition published by Science Press, Beijing, 2010); *Robust and H_∞ Control* (New York: Springer, 2000); *Linear Systems Theory* (Boston: Birkhauser, 2004; Chinese translation published by Tsinghua University Press, 2008); *Hard Disk Drive Servo Systems* (New York: Springer, 1st Edition, 2002; 2nd Edition, 2006); and *Unmanned Rotorcraft Systems* (New York: Springer, 2011). He served/serves on the editorial boards for a number of international journals including *IEEE Transactions on Automatic Control*, *Automatica*, *Systems & Control Letters*, *Asian Journal of Control*, and *Journal of Control Theory and Applications*.

Dr Chen is a Fellow of IEEE. He was the recipient of *Best Poster Paper Award*, 2nd Asian Control Conference, Seoul, Korea (1997); *University Researcher Award*, National University of Singapore (2000); *Prestigious Engineering Achievement Award*, Institution of Engineers, Singapore (2001); *Temasek Young Investigator Award*, Defence Science & Technology Agency, Singapore (2003); *Best Industrial Control Application Prize*, 5th Asian Control Conference, Melbourne, Australia (2004); *Best Application Paper Award*, 7th Asian Control Conference, Hong Kong (2009); and *Best Application Paper Award*, 8th World Congress on Intelligent Control and Automation, Jinan, China (2010).



T. H. Lee received B.A. degree with First Class Honors in Engineering Tripos from Cambridge University, England, in 1980; and Ph.D. degree from Yale University in 1987. He is Professor in the Department of Electrical and Computer Engineering at National University of Singapore (NUS); and also Professor in NUS Graduate School, NUS NGS. He was Past Vice-

President (Research) of NUS.

Dr Lee's research interests are in areas of adaptive systems, knowledge-based control, intelligent mechatronics and computational intelligence. He currently holds Associate Editor appointments in *IEEE Transactions in Systems, Man and Cybernetics*; *IEEE Transactions in Industrial Electronics*; *Control Engineering Practice* (an IFAC journal); and the *International Journal of Systems Science* (Taylor and Francis, London). In addition, he is Deputy Editor-in-Chief of the *IFAC Mechatronics* journal.

Dr Lee was a recipient of Cambridge University Charles Baker Prize in Engineering; the 2004 ASCC (Melbourne) Best Industrial Control Application Paper Prize; 2009 IEEE ICMA Best Paper in Automation Prize; and 2009 ASCC Best Application Paper Prize. He has also co-authored five research monographs (books), and holds four patents (two of which are in the technology area of adaptive systems, and the other two are in the area of intelligent mechatronics). He has published more than 300 international journal papers.

Dr Lee was Invited Panelist at the World Automation Congress, WAC2000 Maui USA; Invited Keynote Speaker for IEEE International Symposium on Intelligent Control, IEEE ISIC 2003 Houston USA; Invited Keynote Speaker for LSMS 2007, Shanghai China; Invited Expert Panelist for IEEE AIM2009; Invited Plenary Speaker for IASTED RTA 2009, Beijing China; Invited Keynote Speaker for LSMS 2010, Shanghai China; and Invited Keynote Speaker for IASTED CA 2010, Banff Canada.